Northumbria Research Link

Northumbria
University
NEWCASTLE

Singlemode-Multimode-Singlemode Fiber Structures for Sensing Applications – A Review

Qiang Wu*, Yuwei Qu, Juan Liu, Jinhui Yuan*, Sheng-Peng Wan, Tao Wu, Xing-Dao He, Bin Liu*,
Dejun Liu, Youqiao Ma, Yuliya Semenova, Pengfei Wang, Xiangjun Xin, Gerald Farrell

(Invited paper)

***Abstract*—A singlemode-multimode-singlemode (SMS) fiber structure consists of a short section of multimode fiber fusion-spliced between two SMS fibers. The mechanism underpinning the operation of an SMS fiber structure is multimode interference and associated self-imaging. SMS structures can be used in a variety of optical fiber systems but are most commonly used as sensors for a variety of parameters, ranging from macro-world measurands such as temperature, strain, vibration, flow rate, RI and humidity to the micro-world with measurands such as proteins, pathogens, DNA, and specific molecules. While traditional SMS structures employ a short section of standard multimode fiber, a large number of structures have been investigated and demonstrated over the last decade involving the replacement of the multimode fiber section with alternatives such as a hollow core fiber or a tapered fiber. The objective of replacing the multimode fiber has most often been to allow sensing of different measurands or to improve sensitivity. In this paper, several different categories of SMS fiber structures, including traditional SMS, modified SMS and tapered SMS fiber structures are discussed with some theoretical underpinning and reviews of a wide variety of sensing examples and recent advances. The paper then summarizes and compares the performances of a variety of sensors which have been published under a number of headings. The paper concludes by considering the challenges faced by SMS based sensing schemes in terms of their deployment in real world applications and discusses possible future developments of SMS fiber sensors.**

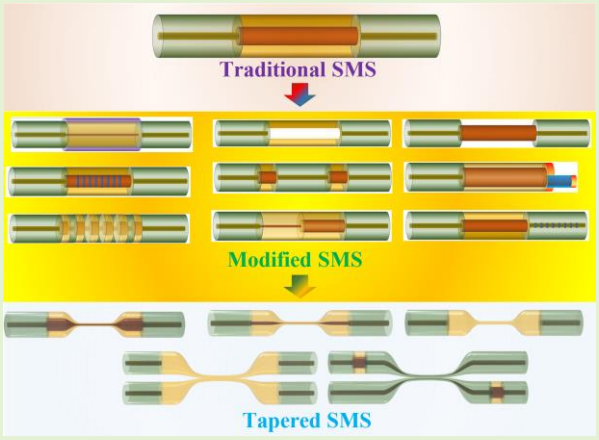

***Index Terms*—SMS, multimode interference, biosensor, chemical sensor, thin-core fiber, small-core fiber, no-core fiber, hollow core fiber, fiber interferometer**

I. Introduction

OPTICAL fiber possesses a number of unique advantages over other transmission media that include small size, light weight, low transmission loss and immunity to interference from electromagnetic fields. Since the first low loss optical silica fiber was proposed in 1960s and fabricated in the 1970s [1-3], the technology has witnessed a wide range of research driven innovations and developments, with a particular focus on applications in communications and sensing, Typically an optical fiber has high refractive index (RI) core surrounded by a lower RI cladding region. Total internal reflection occurs at the core/cladding interface so that light can be transmitted within the optical fiber. If a low loss material such as silica is used, ultralow transmission loss is possible so that the attenuation of the fiber is very small, circa 0.21 dB/km at 1550 nm. The advantage of ultralow transmission loss is that it makes it possible for optical fiber to be used for remote and distributed sensing, for example, to sense environmental perturbations such as temperature, strain

This work was supported by the Natural Science Foundation of Jiangxi Province (Grant No. 20192ACB20031 and 20192ACBL21051); the National Natural Science Foundation of China (Grant No. 62065013, 61665007 and 61465009); Major Discipline Academic and Technical Leaders Training Program of Jiangxi Province, China (Grant No. 20172BCB22012). (The corresponding authors are Qiang Wu, Jinhui Yuan and Bin Liu).

Qiang Wu, Bin Liu, Juan Liu, Sheng-Peng Wan, Tao Wu and Xing-Dao He are with the Key Laboratory of Nondestructive Test (Ministry of Education), Nanchang Hangkong University, Nanchang 330063, China. (e-mail: qiang.wu@northumbria.ac.uk; liubin@nchu.edu.cn). Qiang Wu is also with the Faculty of Engineering and Environment, Northumbria University, Newcastle upon Tyne, U.K.

Yuwei Qu and Xiangjun Xin are with Beijing University of Posts and Telecommunications, Beijing, 100876, China.

Jinhui Yuan is with the Research Center for Convergence Networks and Ubiquitous Services, University of Science & Technology Beijing, Beijing 100083, China. (e-mail: yuanjinhui81@163.com).

Dejun Liu and Pengfei Wang are with the Key Laboratory of Optoelectronic Devices and Systems of Ministry of Education and Guangdong Province, College of Physics and Optoelectronic Engineering, Shenzhen University, Shenzhen, 518060, China.

Youqiao Ma is with School of Physics and Optoelectronic Engineering, Nanjing University of Information Science and Technology, Nanjing, China.

Yuliya Semenova and Gerald Farrell are with Photonics Research Centre, Technological University Dublin, Dublin, Ireland.

and acoustic signals [4-8] over a wide geographical region. There are a wide variety of optical fiber sensors types and structures, for example, based on a fiber grating [9-14], surface plasmon resonance (SPR) [15-17] and fiber interferometers (FIs) [18-20].

An optical FI typically involves multiple beams propagating along multiple separate optical fibers or alternatively along different paths within a single optical fiber, where the multiple beams are transmitted independently but interfere when they are combined. The interference can be either constructive or destructive, resulting in transmission peaks or dips over a wide wavelength range. In an FI based sensor, changes in the local environment, for example due to stress or temperature, change the effective path lengths and thus the spectral position of the peaks or dips, so that the value of an unknown measurand can be determined by measuring changes in the spectrum, such as wavelength, intensity, phase or bandwidth [21]. An optical FI based on multiple fibers needs separate optical devices such as splitters and combiners to allow multiple beam transmission within the different optical fibers to introduce phase differences between these beams. In order to miniaturize an optical FI, in-line structures which utilize multimode interference along a single optical fiber have been proposed [22-23], which are more compact. There are three main types of multimode interferometers (MMI), namely a Fabry-Perot Interferometer (FPI) [24-26], Sagnac Loop Interferometer [27-28] and singlemode-multimode-singlemode (SMS) fiber structures [18, 29-30]. An FPI is composed of two parallel surfaces, with a defined distance between the two surfaces. Light waves travelling between the two surfaces will accumulate a wavelength dependent phase difference and thus interference will occur when the waves meet.

A fiber based FPI can be classified into one of two categories: intrinsic [24] and extrinsic [25] FPI, depending on whether the reflectors are formed inside or outside of fibers. For an intrinsic FPI, the reflecting components are within the fiber, for example in the case of a micro-hole [24], while in an extrinsic FPI the reflecting components lie outside of the fibers, for example where an air gap is placed between two fiber ends [25].

A Sagnac loop is normally formed by an optical fiber loop, where a 3dB fiber coupler divides the input light into two counter-propagating beams and a highly birefringent fiber is placed in the loop. Interference occurs due to the phase difference introduced by transmission along both the slow and fast axes of the highly birefringent fiber.

Finally, an SMS fiber structure utilises a short section of multimode fiber (MMF) spliced between two singlemode fibers (SMFs). An SMS structure is frequently referred to as a fiber heterostructure, given that it will always involve a combination of different fiber types. SMS structures offer some unique advantages such as ease of fabrication, low cost, flexible design and high sensitivity, all of which are useful advantages in the development of real-world sensors.

In this paper, a systematic review of various categories of SMS fiber sensor structures is provided. The first category "Traditional SMS fiber structures", in which the center fiber is an MMF, are considered in Section II, with a summary theoretical underpinning using a mode propagation analysis (MPA) and an overview of the sensing applications of traditional SMS structures. Section III presents "Modified SMS fiber structures" which describes a variety of different heterostructure designs using other types of fibers as an alternative to a simple MMF section. Section IV considers "Tapered SMS fiber structures", which are among the most complex SMS structures, with applications in biosensing and chemical sensing. Section V summarizes and compares the performance and applications of the three categories of SMS fiber structures under the headings of temperature, strain, RI and bio-chemical sensing. Finally, Section VI "Challenges and opportunities" discusses future challenges and likely/future developments for SMS fiber structures.

II. Traditional SMS fiber structures

A simple traditional SMS fiber structure is fabricated by fusion splicing a short section of MMF between two SMFs. Figure 1(a) shows a schematic diagram of an SMS fiber structure [29].

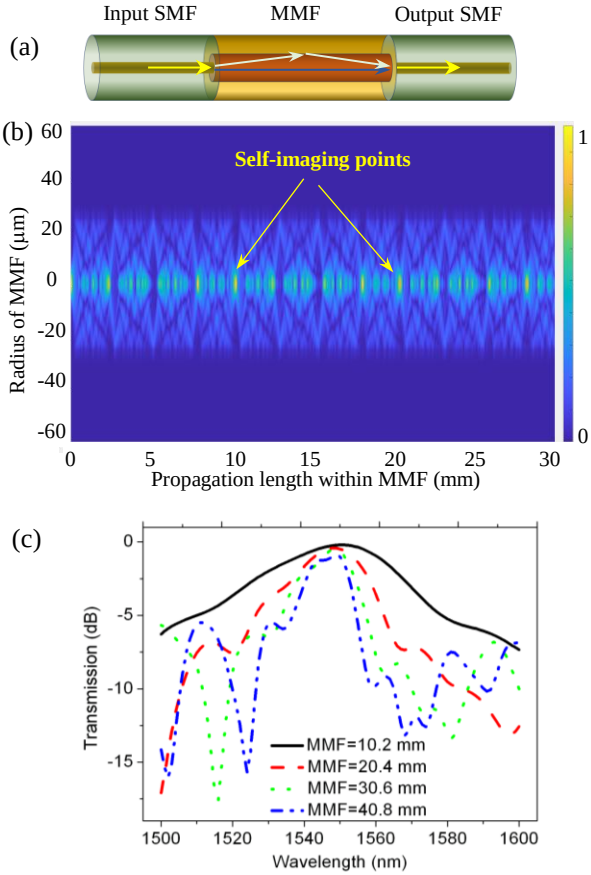

Fig. 1 (a) Schematic diagram of a traditional SMS fiber structure [29], (b) calculated mode distribution along an MMF (length 30 mm) using Eq. (3), and (c) calculated spectral response of an SMS using Eq. (5).

As shown in Fig. 1(a), as light is injected from input SMF into the MMF, multiple modes (including fundamental and higher order modes) will be excited and propagate independently through the MMF section. The MMF can be either a step-index or graded index fiber [31-32]. Multimode interference occurs between these multiple modes within the MMF and this dictates the transmission spectral response at the output SMF. There are various numerical simulation methods

for predicting the spectral response of an SMS fiber structure, such as the beam propagation method (BPM) and modal propagation analysis (MPA). The typical commercial software for BPM is "Rsoft", which is easy to use and is capable of simulating light propagation within complex fiber structures. However for larger-dimension waveguides, with a large number of modes, a BPM simulation can be time consuming if it is to achieve reliable results. MPA is a fast simulation method for simple fiber structures and is particularly suitable for long waveguides.

Assuming that the SMF and MMF are circularly symmetric and the central SMF and MMF axes are aligned perfectly, only the LP_{0m} modes can be excited within the MMF when light is injected from the input SMF into the MMF. In both input and output SMFs only the fundamental guided mode $E_S(r)$ can be supported, which can be decomposed into the eigenmodes LP_{0m} in the MMF when the light enters from the input SMF [18, 29]. Defining the field profile of LP_{0m} as $\varphi_m(r)$ which are the eigenmodes of the MMF (the eigenmodes within MMF are normalized as $\int_0^\infty |E_S(r)|^2 rdr = \int_0^\infty |\varphi_m(r)|^2 rdr = 1, m = 1, 2, ...$), the input field at the MMF is equal to that of the SMF $E_S(r)$, which can be written as [18, 29]:

$$E_S(r) = \sum_{m=1}^{M} b_m \varphi_m(r) \quad (1)$$

where M is the total number of eigenmodes LP_{0m} within MMF, b_m is the excitation coefficient of each eigenmode in the MMF, which is the field overlap between the input SMF $E_S(r)$ and the MMF eigenmode of $\varphi_m(r)$:

$$b_m = \frac{\int_0^\infty E_S(r)\varphi_m(r)rdr}{\int_0^\infty \varphi_m(r)\varphi_m(r)rdr} \quad (2)$$

In the MMF section, the field at a propagation distance z is:

$$E_M(r,z) = \sum_{m=1}^{M} b_m \varphi_m(r)\, exp(j\beta_m z) \quad (3)$$

where β_m is the propagation constant of each eigenmode within the MMF. Assuming the parameters of the output SMF are the same as those of the input SMF, the transmission power of the SMS fiber structure can be determined by using the field overlap integral method between $E_M(r,z)$ and the fundamental mode of the output SMF $E_S(r)$ as

$$P(z) = 10 \cdot log_{10}\left(\frac{\left|\int_0^\infty E_M(r,z)E_S(r)rdr\right|^2}{\int_0^\infty |E_M(r,z)|^2 rdr \int_0^\infty |E_S(r)|^2 rdr}\right) \quad (4)$$

Substituting Eq. (3) into Eq. (4) and utilizing the orthogonal relationship between the eigenmodes of the MMF, the output of the SMS fiber structure can be simplified as:

$$P(z) = 10 \cdot log_{10}(|\sum_{m=1}^{M} b_m^2\, exp(j\beta_m z)|^2) \quad (5)$$

As result of MMI, the well-known self-imaging phenomenon occurs periodically within the MMF [22, 33]. Figure 1(b) shows an example of simulated mode distribution along the MMF section using Eq. (3), where the wavelength is assumed 1550 nm. The results show that the self-imaging length of the SMS fiber structure is circa 10.2 mm.

As the surrounding environmental parameters (temperature, strain, vibration, etc) change, several parameters, such as the effective RI of both the core and the cladding, the length and diameter of the MMF may change, and thus the eigenmodes $\varphi_m(r)$ and effective length of the MMF will change, resulting in changes to b_m in Eq. (2) and the output of the SMS fiber structure defined in Eq. (4-5). Fig. 1(c) is the simulated spectral responses of the SMS fiber structure with different MMF lengths using Eq. (5). In the simulations, the core/cladding RI values of the SMF and MMF are 1.4504/1.4447 and 1.4446/1.4271 respectively, the core diameters of SMF and MMF are 50 and 105 μm and both SMF and MMF are step index fibers. The traditional SMS fiber structure can have a variety of applications but the two most common are as an edge filter or as a stand-alone sensor.

A. Edge filter applications

A traditional SMS fiber structure can be fabricated to implement a bandpass filter spectrum, which can transmit light within a specific wavelength range. Typically, at a spectral edge, the transmission level versus wavelength slope is well defined, repeatable and linear, for example see Fig. 1(c) over the wavelength range from 1550-1560 nm and can be used as the basis of an edge filter for wavelength measurement and sensor system demodulation [34-36]. A ratiometric demodulation system frequently employs an edge filter, where the optical signal is split into two paths: one path contains an edge filter while the other path is used as a reference arm, which can compensate for the power variations due to the perturbations in the optical signal source [37-38]. By measuring the power ratio, the wavelength can be determined.

Edge filter based designs can also be used for sensing, typically using more than one SMS structure and possibly other fibre based devices such as a Fibre Bragg Grating. Figure 2(a) shows a schematic diagram using a pair of SMS fiber structures to measure both temperature and strain simultaneously [39]. In this sensor configuration, strain is applied to SMS-1 only, but both SMS-1 and SMS-2, acting as edge filters, are influenced by the temperature. The wavelength of the laser source is selected to lie within the linear slope range of the two SMS edge filters and a reference arm is used to compensate for source power fluctuations. A strain and temperature resolution of 0.34 με and 0.14 °C respectively have been achieved, with very low strain measurement error (0.39 με) induced by temperature variations from 10 °C to 40 °C.

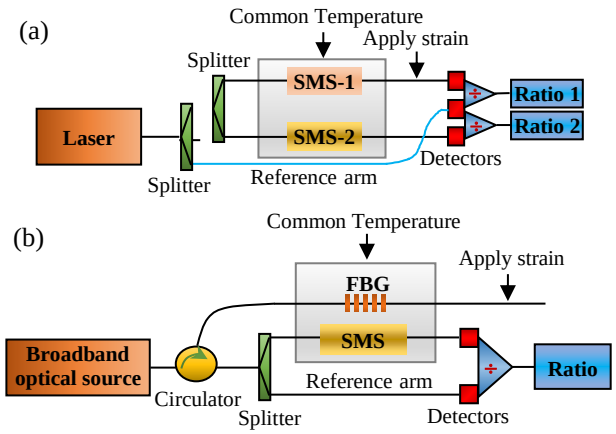

Fig. 2 A schematic diagram of for the ratiometric sensing system using SMS fiber as an edge filter (a) a pair of SMS fiber structures [39] and (b) SMS with FBG [40].

Figure 2(b) shows a combination of an SMS fiber structure with an FBG for simultaneous measurement of both strain and temperature with better than 3.4 με resolution for strain and a small temperature induced error of 34 με in the temperature range from 10 to 60 °C [40].

B. Stand-alone sensor applications

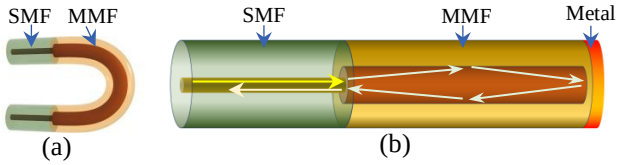

Fig. 3 A schematic diagram of (a) bend [47] and (b) reflective [55] SMS fiber structure

As mentioned above a simple SMS fiber structure itself can be used as a sensor for temperature and strain measurement [41-42]. An SMS fiber structure can also be used in distributed sensing based on an optical time-domain reflector [43] and Brillouin optical time-domain analysis [44].

Up to this point, the SMS structures presented have all been straight but an SMS fiber structure incorporating macro bending is also possible and has been proposed and experimentally investigated. This sensor has a higher temperature sensitivity than a straight SMS fiber sensor [45]. For a bent SMS fiber structure (Fig. 3(a)), the RI distribution within MMF is not symmetric and can be defined by an equivalent RI distribution as follows [46-47]:

$$n = n_0\left(1 + \frac{x}{R_{eff}}\right) \qquad (6)$$

where n_0 is the RI of the straight MMF, x is the distance from the center axis of the MMF and r_{eff} is the equivalent bend radius which can be expressed as follows [29]:

$$r_{eff} = \frac{R}{1-\frac{n_0^2}{2}[P_{12}-v(P_{11}+P_{12})]} \qquad (7)$$

where R is the bend radius of the fiber, v is the Poisson ratio and P_{11} and P_{12} are the components of the photoelastic tensor. Since n is dependent on the bend radius, the output spectrum of the SMS fiber structure is very sensitive to bend radius. A displacement sensor based on a bent SMS fiber structure has been proposed and investigated [48]. The bent SMS fiber structure has also been used as a curvature sensor [49] for vibration sensing [50-51], within a fiber laser [52], for strain sensing [53] and breath state monitoring [54]. Finally, a reflective SMS fiber structure (Fig. 3(b)) has been proposed for liquid-solid phase change monitoring in a phase change material [55] and also as a flow rate sensor [56] utilizing the property of ultra-sensitivity of SMS fiber structures to bend radius.

III. Modified SMS fiber structures

In a traditional SMS fiber structure, multiple propagating modes are confined within the core of the MMF, so given the presence of the cladding there is no direct contact with surrounding environment and hence such structures cannot be readily used for chemical or bio-sensing. In order to address this problem, a large number of investigations have taken place on the modification of a traditional SMS fiber structure to allow an SMS structure to interact with the surrounding environment and allow for bio-chemical sensing. These investigations have significantly stimulated the development of the SMS fiber structure as a sensor. The key idea underpinning the modification of an SMS fiber structure for bio-chemical sensing is excitation of cladding modes within the multimode section so that the surrounding medium may influence the modes. Such modified SMS fiber structures can be classified as: singlemode-no-core-singlemode (SNCS), singlemode-small-core-singlemode (SSCS), singlemode-hollow core-singlemode (SHCS), SMS coupler and combination SMS fiber structures.

A. SNCS fiber structure

A no-core fiber (NCF) is a form of waveguide using only a material with a homogeneous RI. Unlike normal optical fibers, an NCF has no cladding, on the assumption that the surrounding material acts as a cladding of the NCF. Figure 4(a) shows a schematic diagram of an NCF used in an SMS structure to form an SNCS fiber structure [18]. RI changes in the surrounding material will introduce changes in the mode transmission in the NCF and thus alter the output of the SNCS fiber structure.

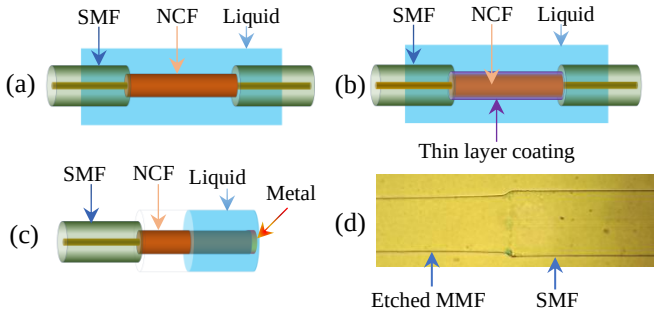

Fig. 4 A schematic diagram of (a) an SNCS [18] and (b) a thin layer coated [70], (c) reflective SNCS [80] fiber structure, and (d) a microscope image of the joint between etched MMF (NCF) and SMF [18]. Reprinted with permission from [18] © The Optical Society.

The MPA method described above for traditional SMS fiber structures can be easily applied to carry out numerical simulations for the SNCS fiber structure, where the cladding is the material surrounding the NCF [18]. An SNCS fiber structure was firstly proposed by Wang *et al*. using an NCF to substitute for the MMF in an SMS fiber structure for RI sensing [57]. A detailed theoretical analysis and experimental investigation was carried out in 2011, in which the NCF was fabricated by wet etching the cladding of a conventional MMF (AFS 105/125Y) using hydrofluoric (HF) acid. The resulting sensor had a maximum RI sensitivity of 1815 nm/ RIU (RI unit) [18]. The RI sensitivity increases as the diameter of NCF decreases, but is independent on the length of the NCF, which provides a possible route to improving the RI sensitivity of such an SNCS fiber structure. However a significant disadvantage is the requirement for the fiber etching process which is dangerous due the use of HF acid. Furthermore accurate control of both the etched fiber diameter and surface roughness is very difficult.

A commercial NCF is an ideal substitute for the etched MMF and thus the use of commercial NCF sections to configure the SNCS fiber structure has been widely investigated. Such SNCS fiber structures have been demonstrated as sensors for: temperature measurement [58-59]; phase transition detection [60]; RI sensing using a V-groove to strengthen mechanical properties [61]; using a fiber ring cavity laser to achieve narrow spectral bandwidth [62]. Multiple NCFs can also be cascaded for multi-point RI measurement [63] and for use with high RI liquids using a leaky mode approach [64]. SNCS fiber structures have also been used as sensors to distinguish fresh and degraded turbine gearbox lubricant oil [65] and to detect the presence of the refrigerant LiBr-H_2O [66].

Coating a high RI material (larger than that of NCF) as a thin layer (Fig. 4(b)) onto the SNCS fiber structure can significantly improve RI sensitivity [67-70]. For example, Xue *et al.* proposed an SNCS fiber sensor for the measurement of surrounding RI with an average sensitivities of 900 and 206 nm/RIU for RI ranges from 1.31 to 1.35 and 1.0 to 1.03 respectively [67], which was further improved to 1199.18 nm/RIU in the RI range from 1.321 to 1.382 [68] with a reflective configuration. The maximum sensitivity of 1277.8 nm/RIU was achieved by optimization of the sensor structure reported in [69-70], and the influence of the coating thickness of its modes has been analysed in [71]. If the SNCS fiber structure is functionalized with a specific material, it can be used for detection of other physical and bio-chemical parameters. The variety of application areas is vast, as testified by these exampole: Li *et al.* sealed ferrofluids in a capillary around the SNCS to measure electric current amplitude with a sensitivity of 2.12 dB/A [72] and Zhang used a U-shaped SNCS with magnetic fluid to measure magnetic field strength with a sensitivity of 3185.2 pm/mT [73]; Wen *et al.* used a ZnO-coated SNCS fiber structure for relative humidity and ethanol detection using a fiber ring laser configuration [74]; Singh *et al.* coated gold nanoparticles (AuNPs), silver nanoparticles (PVA-AgNPs) and graphene oxide (GO) on the NCF to excite surface plasmon polaritons to detect L-Cysteine (L-Cys) molecules [75]; Vicente *et al.* coated SnO_{2-x} on the sensor surface to improve sensitivity and applied the structure to IgG detection with limit of detection (LoD) of 0.6 mg/L [76]; As a final example Cardona-Maya *et al.* used functionalized SNCS to detect goat IgG with LoD of 0.2 mg/L [77].

Finally a reflective SNCS sensor can be implemented by coating a thin metal layer at the end of NCF (Fig. 4(c)), which has potential uses as a sensing probe for in-vivo medical diagnostics. Antonio-Lopez *et al.* used the reflective SNCS fiber structure to detect liquid level [78]; Zhou *et al.* applied such an SNCS fiber sensor to RI measurement with a sensitivity of 141 nm/RIU for an RI circa 1.33 [79], which was further improved to 327 nm/RIU using a small diameter 55 μm NCF by Zhou *et al.* [80] and improved even further by Novais et al. to 1467.69 nm/RIU using a diameter 24 μm NCF [81].

B. SSCS fiber structures

A small core fiber (SCF, also called thin core fiber) can also be used as a substitute for a cladding-etched MMF to form an SSCS fiber structure. In this structure the disparity between the smaller core size of the SCF and the input SMF core diameter means that multiple modes are excited in the cladding of the SCF, so that the SCF in effect acts as a multimode fiber section, but where the external environment acts as the cladding, so that the modes can be directly influenced by the surrounding environment. Several examples of such sensors have been demonstrated: Zhu *et al.* applied an SSCS structure to high temperature (850 °C) measurement with a sensitivity of 18.3 pm/°C [82] while Shi *et al.* cascaded two SSCS for simultaneous measurement of both temperature and strain [83]; Xu *et al.* successfully applied an SSCS to liquid level measurement with a maximum sensitivity of 0.288 nm/mm [84] and Xia *et al.* studied both a transmissive and reflective SSCS for RI sensing [85].

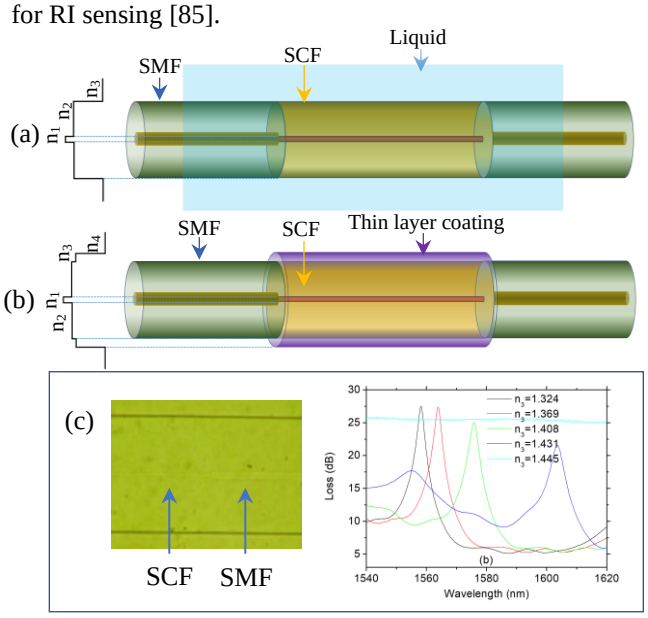

Fig. 5 A schematic diagram of (a) an SSCS [86], (b) a thin layer coated SSCS fiber structure [90], (c) a microscope image of the joint between SCF and SMF, and measured spectral response at different RI value liquid [86]. Reprinted with permission from [86].

Figure 5(a) shows a schematic diagram of an SSCS fiber structure [86]. The MPA method mentioned previously is also suitable for the simulation of the spectral response of an SSCS fiber structure. However, an additional complexity here is that SCF has three layers with different RIs: the small core n_1, the cladding n_2 and the surrounding material n_3, so that the eigenmodes within SCF φ are different from that of a pure NCF. Assuming both the SMF and SCF have a step index profile, the input field at the SCF can be written as [86-88]:

$$\boldsymbol{k_0 n_3 < \beta < k_0 n_2}$$

$$\varphi(r) = \begin{cases} J_0\left(u\frac{r}{a}\right); & r \le a \\ A_1 J_0\left(u'\frac{r}{b}\right) + A_2 Y_0\left(u'\frac{r}{b}\right); & a \le r \le b; \\ A_3 K_0\left(v\frac{r}{b}\right); & r \ge b \end{cases} \quad (6)$$

and

$$\boldsymbol{k_0 n_2 < \beta < k_0 n_1}$$

$$\varphi(r) = \begin{cases} J_0(u\frac{r}{a}); & r \le a \\ A_1' I_0(v'\frac{r}{b}) + A_2' K_0(v'\frac{r}{b}); & a \le r \le b; \\ A_3' K_0(v\frac{r}{b}); & r \ge b \end{cases} \quad (7)$$

where a and b are the radii of the core and cladding of the SCF, J_0, Y_0, I_0 and K_0 are zero order normal and modified Bessel functions respectively, and u, u', v, v', A_1, A_1', A_2, A_2', A_3, A_3' are defined as follows:

$$\begin{cases} u = a\sqrt{k_0^2 n_1^2 - \beta^2} \\ u' = b\sqrt{k_0^2 n_2^2 - \beta^2} \\ v = b\sqrt{\beta^2 - k_0^2 n_2^2} \\ v' = b\sqrt{\beta^2 - k_0^2 n_3^2} \end{cases} \quad (8)$$

$$\begin{cases} A_1 = \frac{\pi}{2}[uJ_1(u)Y_0(u'c) - u'cJ_0(u)Y_1(u'c)] \\ A_2 = \frac{\pi}{2}[u'cJ_1(u'c)J_0(u) - uJ_1(u)J_0(u'c)] \\ A_3 = \frac{1}{k_0(v)}[A_1 J_0(u') + A_2 Y_0(u')] \end{cases} \quad (9)$$

$$\begin{cases} A_1' = [v'cJ_0(u)K_1(v'c) - uJ_1(u)K_0(v'c)] \\ A_2' = [v'cJ_0(u)I_1(v'c) + uJ_1(u)I_0(v'c)] \\ A_3' = \frac{1}{k_0(v)}[A_1' I_0(v') + A_2' K_0(v')] \end{cases} \quad (10)$$

where $k_0 = 2\pi/\lambda$, $c = a/b$, λ is the wavelength of light in a vacuum.

A comprehensive study of the SSCS fiber structure for RI sensing has been undertaken, with a maximum sensitivity of 1815 nm/RIU achieved [86], and this structure has been used for detecting bovine serum albumin (BSA) in phosphate-buffered saline (PBS) [89]. Furthermore, if the SCF is coated with a functionalized thin layer (Fig. 5(b)) [90], the SSCS fiber sensor can be used to detect specific chemical/biological molecules. For example, Gu *et al.* deposited poly(allylamine hydrochloride) and poly(acrylic acid) on the SSCS for pH sensing in either acid or alkali solutions (in the pH range 2.5 to 10) with a resolution of 0.013 pH units [91] and used self-assembly nanocoating to detect metal ions over a wide metal ion concentrations range (10 nM-0.1 M) with a detection limit of 9.6 nM [92]; Engholm *et al.* proposed a means to coat a thin layer of polymer on the SSCS for pH sensing in a wider pH range from 1.95 to 11.89 [93] and Ivanov *et al.* studied the influence of overlays on the SSCS for pH sensing [94]; Yu *et al.* used self-assembly technique to functionalize the SSCS for streptavidin measurement with a LoD 0.02 nM [95]; Huang *et al.* developed a layer-by-layer deposition technique for ammonia in water [96] and in air [97] sensing; Zheng *et al*. successfully used a functionalized SSCS for IgG detection with sensitivity of 10.4 nm/(mg/ml) [98]; Long *et al.* functionalized the SSCS with a monolayer poly-l-lysine (PLL) and single-stranded deoxyribonucleic acid (ssDNA) to detect target DNA molecules [99]; Liu *et al.* demonstrated a copper/graphene oxide (Cu/GO) coated cascade SSCS fiber structure for the detection of hydrogen sulfide with a sensitivity of 4.83 pm/ppm [100]. Functionalizing of a reflective SSCS fiber structure has also been widely studied. A phenylboronic -acid-derivatized poly acrylic acid (PAA-PBA)/ polyvinyl alcohol (PVA) functionalized reflective SSCS fiber tip was reported for glucose detection for physiological (human body) pH levels [101] and a methylcellulose film-coated reflective SSCS for humidity measurement with a maximum sensitivity of 0.133 nm/RH [102]; Wang *et al*. proposed to deposit a thin carbon nanotube layer, which has better compatibility, on the surface of a reflective SSCS for RI sensing [103]; Finally carbon-nanotube (CNT)/polyvinyl alcohol (PVA) was coated on a reflective SSCS for relative humidity sensing by Ma et al [104].

C. SHCS fiber structures

Antiresonant reflecting optical wave-guiding in a hollow core fiber (HCF) was firstly proposed by Duguay *et al.* in 1986 [105]. In an SMS fiber structure, HCF can also be used to substitute for the MMF section to form an SHCS fiber structure in which anti-resonant reflection will be generated. For example, such an approach has been used for temperature insensitive liquid level measurement [106] and as a gas pressure sensor [107]. Figure 6(a) shows a schematic diagram of an SHCS fiber structure [108]. It is noted that, for the sake of clarity, only half of the light rays are illustrated in Fig. 6(a) because the fiber is an axially symmetric cylinder.

As shown in Fig. 6(a), unlike a traditional guided mode optical fiber, when light is injected from the input SMF into the HCF, since the center of the HCF is air, no total internal reflection will take place at the interface between the inner air and cladding, and thus no guided mode is transmitted within the HCF. According to Snell's law, a part of the light will be reflected at each of the boundaries: the inner air/cladding boundary and the cladding/external environment boundary. These reflected light waves experience multiple reflections within the air core of the HCF (orange dotted arrow in Fig. 6(a)) and undergo interference at the output SMF.

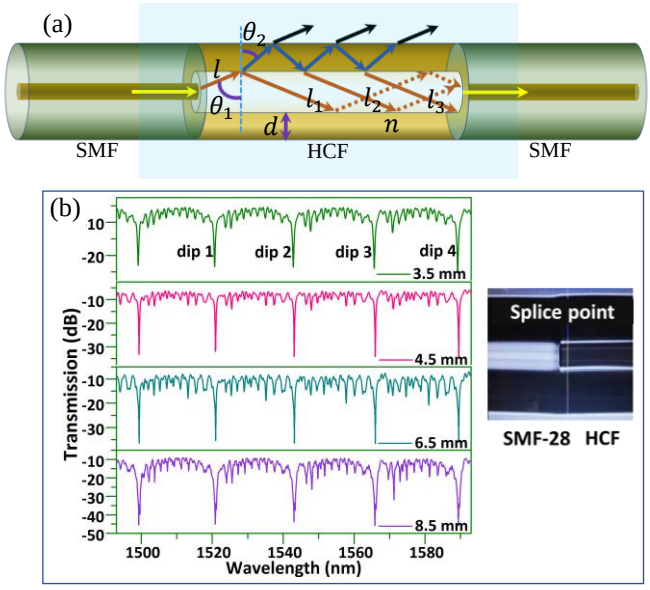

Fig. 6 (a) A schematic diagram and (b) measured spectral responses of the SHCS fiber structure with different HCF lengths and microscope image of splice joint between SMF and HCF [108]. Reprinted with permission from [108].

Assuming the amplitude and angles of refraction of the input light ray l are A, θ_1 and θ_2 respectively (see Fig. 6(a) for the angle definitions) and the RI and thickness of the HCF cladding are d and n respectively, then the phase difference between the two adjacent reflected light rays ($l_1, l_2, l_3, ...$) can be calculated as $\delta = \frac{4\pi}{\lambda} ndcos\theta_2$. The complex amplitudes of the reflected light rays $l_1, l_2, l_3, ...$ are [108-110]:

$$r_1 A, r_2\rho^2 Ae^{i\delta}, r_2(-r_1r_2)\rho^2 Ae^{i2\delta} \cdots, r_2(-r_1r_2)^{m-1}\rho^2 Ae^{im\delta}, \cdots \quad (11)$$

where r_1 and r_2 are the reflection coefficients at the inner air/cladding interface and at the cladding/external environment interface respectively, ρ is the refraction coefficient at the inner air/cladding interface, and m is a positive integer. The amplitude at the output SMF can thus be determined by summing all the reflected amplitudes as follows:

$$\begin{aligned} A_r &= r_1 A + r_2\rho^2 Ae^{i\delta} + r_2(-r_1r_2)\rho^2 Ae^{i2\delta} \\ &\quad + \cdots + r_2(-r_1r_2)^{m-1}\rho^2 Ae^{im\delta} + \cdots \\ &= \frac{r_1 + r_2 e^{i\delta}}{1 + r_1 r_2 e^{i\delta}} A \end{aligned} \quad (12)$$

The light intensity transmitted in the hollow core is hence given as

$$I_r = |A_r|^2 \quad (13)$$

If the hollow core and the outside environment materials are both air, then the values of r_1 and r_2 can be calculated using the Fresnel equations [108]:

$$TE\ mode \quad r_1 = \frac{cos\theta_1 - ncos\theta_2}{cos\theta_1 + ncos\theta_2}, r_2 = -r_1 \quad (14)$$

$$TM\ mode \quad r_1 = \frac{cos\theta_2 - ncos\theta_1}{cos\theta_2 + ncos\theta_1}, r_2 = -r_1 \quad (15)$$

t_1, t_2 are the coefficients of refraction at the interface between the inner air/cladding and cladding/outer air respectively.

$$t_1 = t_2 \quad (16)$$

$$t_1^2 + r_1^2 = 1 \quad (17)$$

As shown in Fig. 6(a), when the length of the HCF is very short, the FP cavity interference between the two ends of the HCF dominates the spectral response. As the length of HCF increases, the influence of antiresonant reflection increases. The transition from FP to antiresonant mechanism has been analyzed by Zheng *et al.* where a critical length for the transition is defined [111]. The advantage of an SHCS fiber structure is its very high quality (Q) factor of the spectral peaks and dips, with a maximum Q factor of 3.3×10^4 achieved experimentally and the extinction ratio and free spectral range are 26 dB and 23 nm respectively [108]. By partially coating silver [110] and uneven platinum [112] on the surface of the HCF, the SHCS fiber structure can achieve very high sensitivity for twist measurement which is strain independent. Cai *et al.* cascaded multiple HCFs with different cladding thicknesses to achieve multipoint temperature sensing [113]. The SHCS fiber structure can also be functionalized for sensing of magnetic field strength [114], humidity [115], hydrogen detection [116], displacement [117], liquid level with sub-micrometer resolution [118] and ultrahigh sensitivity thickness measurement with nanometer resolution [119]. A tailored SHCS fiber structure for RI sensing [120] and Fano resonance achieved by inserting a microsphere into the HCF have also been observed and studied recently [121-122].

D. SMS based couplers

Optical couplers are one of the key components in optical fiber communications system. While the most common approach to coupler fabrication is based on a fused biconical taper, an optical coupler can be also be implemented using two parallel LPGs [123-125], a tilted FBG and a D-shaped fiber [126], or a tapered optical microfiber [127-129]. An SMS fiber structure has multiple transmission bands in the spectrum, which in SMS-based fiber couplers can provide unique spectral filtering properties. For a single SMS fiber structure, at the output SMF, there are both a core mode and cladding modes. In a traditional SMF fiber, only the core mode will be transmitted because cladding modes will be attenuated over a relatively short distance by absorption within the SMF fiber cladding and also by the polymer protection coating, where it is present. If two SMS structures are placed in close parallel, proximity as shown in Fig. 7, then cladding modes will be coupled from the SMS-1 structure to the SMS-2 structure. These cladding modes will be coupled to the MMF-2 and transmit as the core mode in the output SMF-4, effectively coupling Port 1 to Port 4, so that this parallel SMS fiber structure pair can thus act as a fiber coupler [130].

The simulation for the individual SMS-1 and SMS-2 is the same as that in a traditional SMS fiber structure from Eq. (1)-(5). However, at the output SMF-2, not only the core mode, but also cladding modes exist. Assume that the core and cladding modes within the SMF are $E_S(z)$ and $E_C(z)$, and the lengths of MMF-1 and MMF-2 are L_1 and L_2, respectively. Furthermore, assume all the SMFs and MMFs in both the SMS fiber structures have the same parameters. The field distributions for the core mode $E_{S1}(r, L_1)$ and cladding modes $E_{C1}(r, L_1)$ at the start point of SMF-2 can thus be written as [130]:

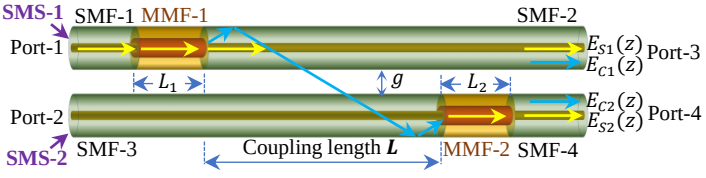

Fig. 7 A schematic diagram of a SMS fiber coupler [130].

$$E_{S1}(r, L_1) = \sum_{m=1}^{M} b_m \varphi_m(r)\, exp(j\beta_m L_1) \quad (18)$$

$$E_{C1}(r, L_1) = b_n \Phi_n(r) \quad (19)$$

where M and b_m are the total number of modes and the excitation coefficient of each eigenmode in the MMF-1 section respectively, which can be calculated using Eq. (2); b_n is the excitation coefficient to the cladding modes in SMF-2 and can be calculated as:

$$b_n = \frac{\int_0^\infty E_{S1}(r,L_1)\Phi_n(r)rdr}{\int_0^\infty \Phi_n(r)\Phi_n(r)rdr} \quad (20)$$

where $\Phi_n(r)$ is the n^{th} mode within SMF-2 ($n = 1$ represents the core mode, $\Phi_1(r) = E_{S1}(r)$ and $n > 1$ represents cladding modes). The mode fields above are normalised as [129]:

$$\int_0^\infty E_{S1}(r)E_{S1}(r)rdr = \int_0^\infty \varphi_m(r)\varphi_m(r)rdr = \int_0^\infty \Phi_n(r)\Phi_n(r)rdr = 1 \quad (21)$$

In the coupling region L, assuming there is no mismatch between the propagation constants of SMF-2 and SMF-3, the fields of the n^{th} cladding modes in SMF-2 and SMF-3 at position $L_1 + L$ can be expressed as [131]:

$$E_{C1n}(r, L_1 + L) = E_{C1n}(r, L_1)\, cos(\, b_n^{'} L) \quad (22)$$

$$E_{C2n}(r, L_1 + L) = -jE_{C2n}(r, L_1)\, sin(\, b_n^{'} L) \quad (23)$$

where $b_n^{'}$ is the evanescent field coupling coefficient of the n^{th} cladding mode between SMF-2 and SMF-3 which can be written as [132]:

$$b_n^{'} = \frac{\sqrt{2\Delta}}{a_0}\frac{U_n^2}{V_n^3}\frac{K_0[W_n(2+g/a_0)]}{K_1^2(W_n)} \quad (24)$$

where a_0 and g are the radius of the fiber cladding and the separation between the SMS-1 and SMS-2 (shown in Fig. 7), respectively, K_0 and K_1 are the modified Bessel functions, Δ is the relative RI difference between the fiber cladding (n_c) and surrounding medium (n_s). $U_n = \frac{2\pi a_0}{\lambda}\sqrt{n_c^2 - N_n^2}$, $V_n = \frac{2\pi a_0}{\lambda}\sqrt{n_c^2 - n_s^2}$ and $W_n = \frac{2\pi a_0}{\lambda}\sqrt{N_n^2 - n_s^2}$ are the normalized parameters and N_n is the effective RI of the n^{th} cladding mode.

The cladding modes $E_{C2n}(r, L_1 + L)$ in SMF-3 will then be coupled to core modes $\varphi_m$within MMF-2, which is given by:

$$E(r, L_1 + L + L_2) = \sum_{m=1}^{M} b_m^* \varphi_m(r)\, exp(j\beta_m L_2) \quad (25)$$

where

$$b_m^* = \sum_{n=2}^{N} \frac{\int_0^\infty E_{C2n}(r,L_1+L)\varphi_m(r)rdr}{\int_0^\infty \varphi_m(r)\varphi_m(r)rdr} \quad (26)$$

$E(r, L_1 + L + L_2)$ will be coupled to the core mode within SMF-4 which is the output of the coupler [149]:

$$E_{S2}(r, L_1 + L + L_2) = \frac{\int_0^\infty E(r,L_1+L+L_2)\Omega(r)rdr}{\int_0^\infty E_{S2}(r)E_{S2}(r)rdr} \quad (27)$$

Equation (27) defines the characteristics of the light coupled from port 1 to port 4. A detailed analysis of the SMS fiber coupler has been provided by Wu *et al.* with an experimentally demonstrated maximum coupling efficiency of 5.9% [130]. The coupling between an SMS fiber structure and an LPG has been also studied with a demonstrated 3 dB bandwidth of 42 nm [133].

E. Combinations of SMS fiber structures

Based on the above SMS fiber structures, there are many reports which involve combinations an SMS fiber structure with other fiber structures to achieve unique properties, such as multiple parameter measurement, sensitivity improvement, etc.

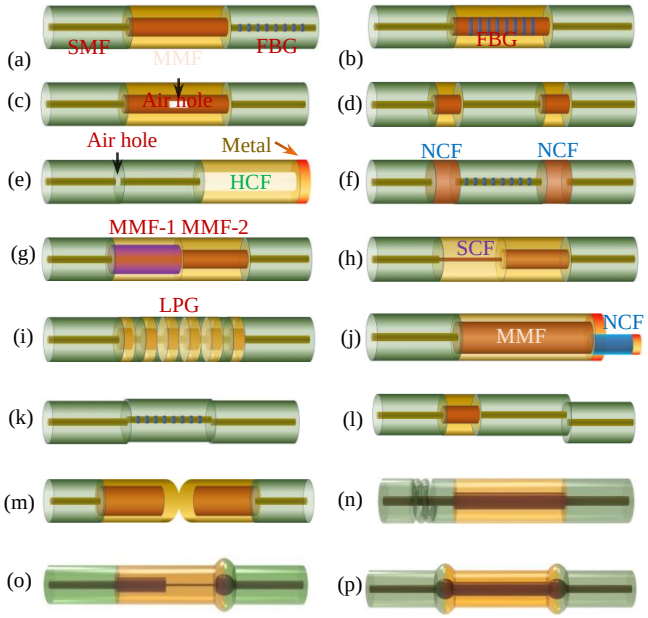

Fig. 8 A schematic diagram of different combined SMS fiber structures: (a) MMF+FBG in SMF [134], (b) FBG in MMF [138], (c) air hole in MMF [141], (d) SMSMS [143], (e) SMF sandwiched between air hole and HCF [146], (f) FBG between two NCF [147], (g) MMF-1+MMF-2 [148], (h) SCF+MMF [151], (i) LPG [155], (j) reflective MMF+NCF [160], (k) core-offset FBG [161], (l) SMS+core-offset SMF [163], (m) round shape [170], (n) twist in input SMF [171], (o) MMF+SCF waist-enlarged [172] and (p) both ends waist-enlarged MMF [173].

Figure 8 summarizes several typical combinations of SMS fiber structures with other fiber structures. In 2011, Wu *et al.* proposed a cascade consisting of an FBG and a traditional SMS fiber structure (Fig. 8(a)) to excite both core and cladding Bragg wavelengths for simultaneous measurement of RI and temperature [134]; The MMF can also be replaced by an NCF [135-136] or the FBG could be replaced by an LPG for multiple parameter measurement with improved sensitivity [137]; an FBG inscribed within a centre section MMF (Fig. 8(b)) is also possible and has also been studied for simultaneous measurement of temperature and other parameters such as strain or bending [138-140].

Physical modification of the structure is also possible. For example, Lin *et al.* drilled a micro hole in the MMF (Fig. 8(c)) to measure gas pressure with sensitivity of -82.131 nm/MPa [141]. In an alternative version [142] the MMF was divided in two halves with air gap between the MMF ends, for application in a tunable laser. Yin *et al.* proposed an SMSMS (Fig. 8(d)) fiber structure for temperature and strain measurement with an axial strain and temperature sensitivity of 0.7096 pm/με (0~2000 με) and 44.12 pm/°C (10~70 °C), respectively [143], which is effectively a reflective SMS fiber structure [144-145]; a Dual-cavity Fabry-Perot interferometer based on an air hole and an HCF (Fig. 8(e)) was also proposed by Gao *et al.* [146] for temperature and high pressure measurement, with high temperature and pressure sensitivities of 19.8 nm/°C and 98 nm/MPa respectively.

Li *et al.* proposed the insertion of an FBG between two SNCS structures (Fig. 8(f)) to achieve simultaneous measurement of both temperature and RI with RI and

temperature sensitivities of 5.85 nm/RIU and 8.72 pm/°C, respectively [147]; two different MMFs were cascaded in an SMS fiber structure (Fig. 8(g)) proposed by Wu *et al.* for simultaneously measurement of both strain (sensitivity of 0.35 pm/με) and temperature (sensitivity of 11.16 pm/°C) [148] with a further study of the structure provided by Bhatia *et al.* [149-150]; an SCF cascade with an MMF (Fig. 8(h)) has been be used for water level, RI, temperature and strain sensing [151] and an alternative structure consisting of an SCF cascaded with a cladding etched MMF was proposed for RI sensing with a sensitivity of 148.27 nm/RIU [152].

Several studies have been carried out involving a combination of an LPG with an SMS fiber structure [153-154], and some interesting research has been undertaken to fabricate an LPG using fusion splices at precise intervals with different types of fibers, such as MMF and SMF (Fig. 8(i)) [155-158], MMF and NCF [159].

A reflective comb filter was proposed using a cascade of an MMF and a small core NCF (Fig. 8(j)) demonstrating a variable extinction ratio from 6 to 11.1 dB [160]. The deliberate use of misalignment of the SMF and MMF fibers in an SMS structure has also been widely investigated, for example, an SMF core-offset spliced between two SMFs (Fig. 8(k)) [161-162], SMS misaligned with output SMF (Fig. 8(l)) [163-166], S-shaped core-offset connection [167-168] and the use of an air gap between the SMS and SMF [169].

Finally, modifications of the fibers to modulate modes in the SMS fiber structures have also been investigated, such as polished shape ends in a split MMF (Fig. 8(m)) [170], a twist in the input SMF (Fig. 8(n)) [171], waist-enlarged SMS fiber structures (Fig. 8(o-p)) [172-173], a spiral microstructure SMS [174], in-line tapers [175-177] and a side-polished fiber [178].

IV. Tapered SMS fiber structure

It is well known that fiber tapers and microfibre couplers are an effective way to reduce fiber diameter and with it increase the interaction between the evanescent field in the fiber and the surrounding environment. This is turn can lead to a substantial increase in sensitivity which is why fiber tapering is now very commonly used as the basis for novel sensors and communications devices. Tapering of an SMS structure is also possible and can be classified into two categories: a tapered SMS fiber structure and a tapered SMS fiber coupler.

A. A tapered SMS fiber structure

In 1997 Knight *et al.* demonstrated for the first time a reduction of the standard optical fiber diameter down to several micrometers by tapering [179], while Tong *et al.* developed an improved tapering technique capable of drawing a fiber with a diameter as low as 50 nm [180]. With such a small diameter the interaction of the optical fiber's evanescent field with the surrounding environment significantly increases with it the capability to be used as a sensor. The research in [18] demonstrated that a cladding-etched SMS fiber structure with a smaller diameter has a higher RI sensitivity than a traditional SMS structure. Tapering of SMS fiber structure has the potential for improving its RI sensitivity even further, whilst avoiding the safety issues associated with etching and also ensuring a low level of surface roughness. Figure 9(a-e) shows five different types of tapered SMS fiber structures.

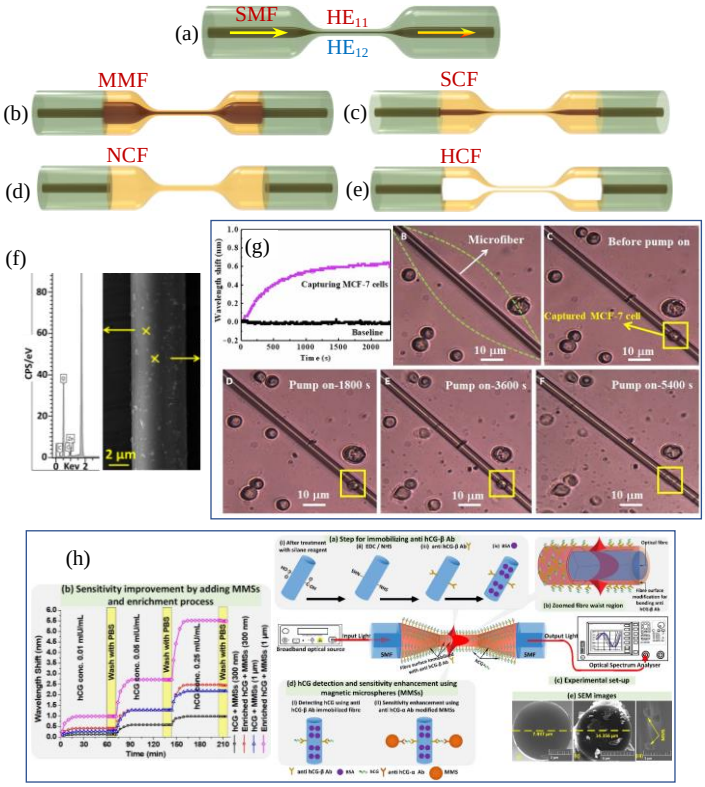

Fig. 9 A schematic diagram of different single tapered (a) SMF [181], (b) SMS [194], (c) SSCS [201], (d) SNCS [205], (e) SHCS [212] fiber structure, (f) SEM image of Nile red coated tapered SCF [204], (g) single molecule detection of biomarker and localized cellular photothermal therapy [193], (h) tapered SNCS for ultrahigh sensitivity detection of hCG with signal amplification of magnetic microspheres [210]. Reprinted with permission from [204], [193] and [210].

In a tapered SMF (Fig. 9(a)), when the taper is nonadiabatic, not only the fundamental mode HE_{11}, but also several higher order modes will be excited, with most of the light energy coupled into HE_{11} and HE_{12}. The two modes will interfere as they travel within the tapered section, resulting in a series of transmission peaks and dips over a wide wavelength range [181]. This phenomenon has been used as the basis of a flowmeter [182] and an RI sensor [183-185]. An ultrashort-waist nonadiabatically tapered SMF was reported with a waist length and diameter of 2.4 mm and 7 μm respectively, and a maximum sensitivity of 25667 nm/RIU has been achieved [186]. The tapered SMF has been combined with an MMF to achieve simultaneous measurement of both temperature and RI [187]. A nonadiabatically tapered SMF can be functionalized for bio/chemical sensing, such as anti-gliadin antibodies [188], glucose detection [189], enzyme-linked immunosorbent assay reader [190], carcinoembryonic antigen-related cell adhesion molecules detection [191], microRNA quantification [192], and biomarker detection in a single molecule [193].

As mentioned previously, a traditional SMS fiber structure cannot readily detect changes in the surrounding RI since light

is trapped within the MMF core, and thus cannot interact with the surrounding environment. Tapering the MMF to a smaller diameter will excite cladding modes in the tapered section and thus can be used for RI sensing. In a tapered SMS fiber structure (Fig. 9(b)), independent of whether the taper is nonadiabatic or not, interference is always observed due to the existence of multimode interference within the MMF section, and thus tapering of SMS fiber structure is relatively simple. A tapered SMS fiber structure was firstly realized by Wang *et al.*, with a demonstration of its use as a high sensitivity RI sensor [194]. In a further refinement the tapered SMS fiber structure was cut in half at the taper waist of the MMF and a thin layer of gold was coated at the end of the tip for use as a high temperature sensor [195]. A tapered SMS fiber structure can also be used for strain [196] and acoustic sensing [197]. The MMF section can also possess an elliptical cross section [198], a bent shape [199] or be side polished [200] etc.

Not all tapers are gradual, for example Shi *et al.* used an electric arc to generate an abrupt taper in an SSCS fiber structure for RI sensing. [201], Liu *et al.* fabricated a tapered SSCS fiber structure (Fig. 9(c)), which has ultrahigh RI sensitivity of 19212.5 nm/RIU [202]. The tapered SSCS fiber was then functionalized with sol gel for ammonia sensing [203], simultaneous measurement of methanol and ethanol concentration [204] and DNA detection with an S-tapered configuration [205].

Tapered SNCS fiber structures (Fig. 9(d)) have been analysed in detail [206]. In 2018, Tian *et al.* proposed a high sensitivity temperature sensor based on a tapered SNCS fiber structure and surrounded with alcohol within a silica capillary, where a maximum temperature sensitivity of 0.49 dB/°C has been achieved [207]. In 2019, Zhang *et al.* proposed an RI sensors based on a tapered SNCS fiber structure (waist diameter 13 μm) with RI sensitivity of 686 nm/RIU within the RI range of 1.333–1.350 [208]. In 2020, Wang *et al.* further proposed a folded-tapered SNCS fiber structure for simultaneous measurement of both RI (1191.5 nm/RIU) and temperature (0.0648 nm/°C) [209]. A functionalized tapered SNCS was used for human chorionic gonadotropin (hCG) detection, where an ultrahigh sensitivity was achieved with a detection limit of 0.0001 mIU/mL [210]. An SHCS fiber structure (Fig. 9(e)) was studied by Zhao *et al.* using a butterfly shaped taper for vibration measurements [211]. Chen *et al.* functionalized a tapered SHCF for hCG detection with an LoD of 0.6 mIU/mL [212]. The tapered section can also utilise a variety of other types of fibers, such as a few mode fiber [213-215], a photonic crystal fiber [216], a ring core fiber [217], a microstructured fiber [218], a side-polished fiber [219] and a dual side hole fiber [220].

Multiple tapers cascaded together and sandwiched between two SMFs, are also possible. For example, in [221] an RI sensor based on a multi-tapered SMS fiber structure was proposed. The sensor is realized by fabricating several tapers in the multimode fiber part of the SMS fiber structure. With eight tapers, an RI sensitivity of 261.9 nm/RIU in the RI range of 1.3333-1.3737 was achieved.

Another RI sensor involving multiple tapers utilised a periodically tapered SCF sandwiched between two SMFs, with the tapers periodically fabricated along the small core fiber using a focused CO_2 laser beam. An average sensitivity of 226.6 nm/RIU was experimentally achieved in the RI range from 1.33 to 1.38 [222].

B. *Tapered SMS fiber coupler*

As mentioned previously, an optical fiber coupler is one of the most important components in many optical fiber systems. The basic principle of an optical fiber coupler is the evanescent field coupling between two optical fibers in physical contact as explained in Section III. If two SMS fiber structures which are physically in contact each other are also tapered to a small diameter, then strong evanescent filed coupling between the two SMS fiber structures will take place. Importantly this structure is suitable for sensing due to the strong evanescent field and sensitivity of the coupling to the local environment. Such tapered SMS fiber couplers can be classified as: a tapered SMF coupler (Fig. 10(a), typically called a microfiber coupler (MFC)); a tapered SNCS coupler (Fig. 10(b)) and a tapered SMS fiber coupler (Fig. 10(c)).

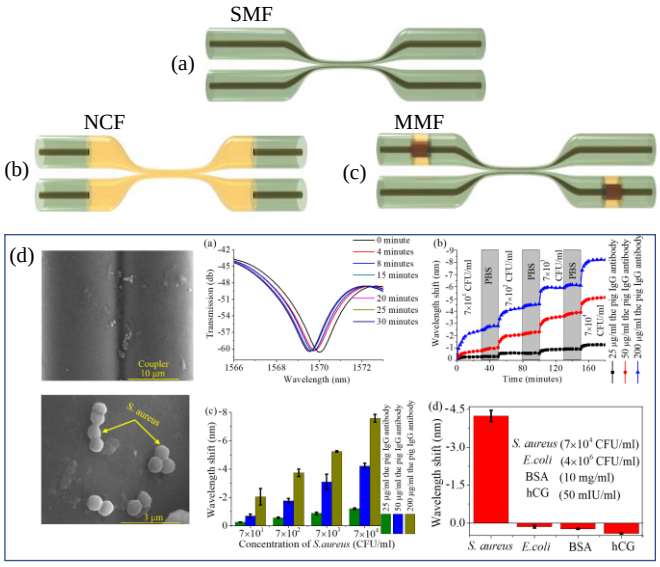

Fig. 10 A schematic diagram of tapered (a) SMF [226], (b) SNCS [245], (c) SMS fiber coupler [246] and (d) tapered SNCS for *S. aureus* measurement [245]. Reprinted with permission from [245].

As an example a tapered SMF coupler was fabricated by placing two traditional SMFs in parallel in physical contact and then heating and stretching the two SMFs with small diameters in the order of few micrometers [223-225]. The resulting tapered SMF coupler has been used for sensing applications, including temperature [226-227], RI [228-230], strain [231], liquid flow rate [232] and magnetic field sensing [233-237] etc. The functionalization of tapered SMF couplers enables the sensors to be used to detect bio-chemical materials, such as humidity [238-239], ammonia [240], ethanol [241], human cardiac troponin, in which the Vernier effect was utilized to improve sensor sensitivity [242], airborne contaminants [243], myocardial infarction I [244].

Most recently tapered SNCS [245] and SMS fiber couplers [246] have been proposed with additional advantages such as

mechanical stability and a ability to measure multiple parameters. For example, two parallel aligned SNCS fiber structures were tapered to small diameters to form a coupler structure, which achieved ultra-high sensitivity label-free quantification of inactivated *Staphylococcus aureus* (*S. aureus*) with an LoD of 3.1 CFU/mL [245] and a tapered SMS fiber coupler has been applied to detect hCG with a minimum concentration of 0.05 mIU/mL [246].

V. Summary

SMS fiber structures can be grouped into three generic categories: traditional SMS; modified SMS and tapered SMS fiber structures, all of which have been discussed in this paper. Traditional SMS fiber structure-based sensors are mainly used for measurements of macro-parameters, such as temperature, strain and displacement. A modified SMS fiber sensor can be used for the measurement of multiple parameters. The tapered SMS fiber structure has a much higher sensitivity, particularly to the surrounding RI and thus is an ideal candidate for bio-chemical sensing applications.

For the purpose of comparison, Table 1 summarizes the typical temperature sensing performance of the three categories of SMS fiber structures.

Table 1 Typical temperature sensing performance of different SMS fiber structures

Fiber structure	Temperature Sensitivity	Detection range	Ref
SMS	84.38 pm/°C	20 ~ 100 °C	[41]
Bent SMS	31.97 pm/°C 0.1 pm°C	20 ~ 80 °C 45 ~ 80 °C	[45]
SNCS+E7	6.5 nm/°C	51 ~ 65 °C	[58]
SNCS+polymer cladding	1.4 dB/°C 15 nm/°C	below 61 °C above 72 °C	[59]
SSCS	18.3 pm/°C	25 ~ 850 °C	[82]
SHCS	33.4 pm/°C	25 ~ 1000 °C	[108]
Tapered SMS +Gold layer	-11.4 pm/°C	0 ~ 1089°C	[195]
Tapered SNCS	0.49 dB/°C	20 ~ 45°C	[207]
Tapered SMF coupler	36.59 pm/°C	0 ~ 1000 °C	[224]
Tapered SMF coupler	11.96 pm/°C	0 ~ 1283 °C	[225]

As can be seen from Table 1, the three categories of SMS fiber structures have similar temperature sensitivities. Tapered SMS fiber sensors do not have any sensitivity advantage over other types of SMS fiber sensors.

Table 2 summarizes the strain sensing performances of the three types of SMS fiber structures, showing that tapered SMS fiber structures have relatively larger sensitivities to strain compared to those of the other two categories of SMS fiber structures.

Table 2 Typical strain sensing performance of different SMS fiber structures

Fiber structure	Strain Resolution	Strain Sensitivity	Detection range	Ref
SMS + FBG	3.4 με	-	0~1667 $\mu\varepsilon$	[39]
SMS 1+SMS 2	0.34 με	-	0~1000 $\mu\varepsilon$	[40]
SMS+ OTDR	< 10 με	-	0~1000 $\mu\varepsilon$	[43]
SSCS	-	-1.03 pm/με	0~1333.3 $\mu\varepsilon$	[83]
SHCS	-	0.61 pm/με	0~1200 $\mu\varepsilon$	[112]
SMMS	-	0.35 pm/με	0~1556 $\mu\varepsilon$	[148]
S-tapered SMS	0.2 με	-103.8 pm/με	0~170 $\mu\varepsilon$	[168]
Polished shape MMF	-	-2.6 pm/με	0~1000 $\mu\varepsilon$	[170]
Tapered SMS	-	-9.536 pm/με	0~160 $\mu\varepsilon$	[196]
Tapered SHCS	-	13.96 pm/με	0~1111.1 με	[213]

Table 3 summarizes the typical RI sensitivity of the different types of SMS fiber structures. The results show that tapered SMS fiber structures have an almost ten times higher RI sensitivity compared to those of the other two categories of SMS structures.

Table 3 Typical RI sensing performance of different SMS fiber structures

Fiber structure	Maximum RI sensitivity	Detection range	Ref
SNCS+TiO2/PSS thin film	1199.18 nm/RIU	1.321 ~ 1.382	[68]
SNCS+RI thin-film	1277.8 nm/RIU	1.333 ~ 1.36	[69]
SNCS	1815 nm/RIU	1.42 ~ 1.437	[18]
SNCS+Liquid+Gold layer	327 nm/RIU	1.33 ~ 1.38	[80]
SSCS	1808 nm/RIU	1.324 ~ 1.431	[86]
SHCS	1684 nm/RIU	1.3360 ~ 1.4365	[120]
SMS+FBG	7.33 nm/RIU	1.324~ 1.439	[134]
Tapered Microfiber	25667 nm/RIU	1.4145 ~ 1.4157	[186]
Tapered SMS	1900 nm/RIU	1.33 ~ 1.44	[194]
Tapered SSCS	19212.5 nm/RIU	1.4304 ~ 1.4320	[202]
Tapered SNCS	686 nm/RIU	1.333 ~ 1.350	[208]
Tapered SHCS+Etched	2565.2 nm/RIU	1.335 ~ 1.400	[214]
Tapered SHCS+Side polished	151.29 nm/RIU	1.3450 ~ 1.4050	[219]

Given the higher RI sensitivity of tapered SMS fiber structures, tapered structures have been widely used for bio-chemical sensing. Table 4 compares the chemical and biological sensing performance of different SMS fiber structures. It is important to note that unlike the comparison tables for other measurands above, in this case the measurands or sensing targets are varied, thus care must be exercised when making comparisons of sensing performance, since for example the type of functional coating used on the sensor may have a significant influence on the performance of the sensor, in addition to the influence of the nature of the underlying SMS structure.

Table 4 Chemical and biological sensing performance of different SMS fiber structures

Fiber structure	Detection parameters	Sensitivity	Detection limit	Ref
SMS+ZnO coated	Relative humidity	0.06 nm/%RH	-	[74]
SMS+SPR	L-Cysteine	0.0009 nm/μM	126.6 μM	[75]
MCM+SnO_{2-x} film	Anti-mouse-IgG		0.6 mg/L	[76]
TCFMI	pH	0.013 pH unit	-	[91]
TCFMI+P4VP+PAA	Metal ion	-	9.6 nM	[92]
SMF–TCSMF–SMF	Streptavidin	0.55 nm /(ng/mm^2)	0.02 nM	[95]
TCSMF MZI	IgG	82.7 nm/RIU	10.4 nm/(mg/ml)	[98]
TCF+MC film-coated	Relative humidity	0.224 dB/%RH	-	[102]
Multimode microfiber	Glucose	1.74 nm(mg/ml)	-	[189]
Tapered SMF+Au nanosphere	CEACAM5 in Serum	0.86 nm/lg M	5.27×10^{-16} M	[191]
Tapered SMF	Single-molecule detection of biomarker	1.45 nm/Log M	6.72 zM	[193]
Tapered SMS coupler (MFC)	Ethanol Methanol	−0.130 nm/ppm −0.036 nm/ppm	~ 77 ppb ~ 281 ppb	[204]
Tapered SNCS	Human chorionic gonadotropin	98 nm/mIU/mL	0.0001 mIU/mL	[210]
Tapered SHCF	Human chorionic gonadotropin		0.6 mIU/ml	[212]
MFC+PMMA	Ethanol Gas	0.65 pm/ppm	-	[238]
MFC+Silica Gel	Ammonia Gas	2.23 nm/ppm	-	[239]
MFC+mesoporous silica coating	Airborne molecular contaminants	0.541 nm /(mg/m^3)	36.7 μg/m^3	[241]
OMC	CTnI		2 fg/mL	[242]
Tapered SNSFC	Staphylococcus aureus		3.1 CFU/mL	[243]

VI. Challenges and Opportunities

SMS fiber structures have attracted tremendous research interest since they were first proposed [22, 33]. Sensors based on SMS fiber structures have been studied for macro-parameter sensing, such as temperature, strain, vibration, phase change and also for micro parameter sensing and detection, including hCG, DNA, glucose, IgG, enzyme assays, foodborne pathogens, microRNA, carcinoembryonic antigens, and biomarkers of single molecules, etc. Compared to other types of sensors, tapered SMS fiber structures have the advantages of high sensitivity and relatively good stability. The applications of SMS fiber structures in biochemical sensing and medical diagnostics for human health monitoring are likely to be key areas for further development. As an example such development will be driven by societies increasing need for rapid testing for diseases, which has seen the development of "lab-on-a-chip" combinations of sensors arrays and microfluidics. Due to the unique advantages of SMS fiber sensors, such as high sensitivity and low cost, it is possible to predict a bright future for the commercialization of such sensors.

However, for practical sensing applications, there are a number of challenges. At an individual sensor level, improvements are needed in reproducibility, repeatability, long term stability and large scale fabrication. At a system level, a common weakness of optical fiber sensing in general is the lack of standards, which means end-users are unable to reliably source different elements of a system from different vendors and be confident that the elements will work well together. A key to the success of optical fibers in optical communications was and remains the high level of standardization in place. Significant progress in standardization has been made for more mature sensing technologies such as FBG sensors but for SMS-based sensors much work remains to be done on standardization.

Miniaturization is a challenge but also is an opportunity for a wider commercialization of SMS fiber sensors. Innovative designs aimed at minimizing the length of the MMF section, the use of a reflective sensor tip to form very compact sensor probes and integration with optofluidic platforms are some of the effective methods to facilitate miniaturization of the sensors.

Future opportunities in research on SMS fiber structures will include studies which seek to integrate SMS fiber sensors with microfluidic systems to stabilize the sensors and to realize lab-on-a-chip sensing; the development of ultrahigh sensitivity sensors for single cell level detection and the application for ex-vivo and in-vivo diagnosis.

Finally, while SMS sensors can justifiably claim to be generally low in cost, the interrogation systems are complex and expensive, frequently requiring an optical spectrum analyser, for example. In the future, development of smart low-cost demodulation systems is needed if SMS sensors are to be widely deployed.

REFERENCES

[1] K. C. Kao and G. A. Hockham, "Dielectric-fibre surface waveguides for optical frequencies," Proc. IEE, vol. 113, no. 7, pp. 1151–1158, 1967.

[2] F. P. Kapron, D. B. Keck, and R. D. Maurer, "Radiation losses in glass optical waveguides," Appl. Phys. Lett., vol. 17, no. 10, pp. 423–425, 1970.

[3] D. B. Keck, R. D. Maurer, and P. C. Schultz, "On the ultimate lower limit of attenuation in glass optical waveguides," Appl. Phys. Lett., vol. 22, no. 7, pp. 307–309, 1973.

[4] M. K. Barnoski et al., "Optical time domain reflectometer," Appl. Opt., vol. 16, no. 9, pp. 2375–2379, 1977.

[5] A. H. Hartog, A. P. Leach, M. P. Gold, "Distributed temperature sensing in solid-core fibers", Electronics Letters, vol. 21, no. 23, pp. 1061-1062, 1985.

[6] T. Kurashima, T. Horiguchi, and M. Tateda, "Distributed-temperature sensing using stimulated Brillouin scattering in optical silica fibers," Opt. Lett., vol. 15, no. 18, pp. 1038–1040, 1990.

[7] R. Bernini, A. Minardo, and L. Zeni, "Dynamic strain measurement in optical fibers by stimulated Brillouin scattering," Opt. Lett., vol. 34, no. 17, pp. 2613–2615, 2009.

[8] D. Milne, A. Masoudi, E. Ferro, G. Watson, L. Le Pen, "An analysis of railway track behaviour based on distributed optical fibre acoustic sensing", Mechanical Systems and Signal Processing, vol. 142, article number: 106769, 2020.

[9] K. O. Hill, Y. Fujii, D. C. Johnson, and B. S. Kawasaki, "Photosensitivity in optical fiber waveguides: Application to reflection filter fabrication," Appl. Phys. Lett., vol. 32, pp. 647–649, 1978

[10] A. D. Kersey, M. A. Davis, H. J. Patrick, M. LeBlanc, K. P. Koo, C. G. Askins, M. A. Putnam, F. J. Friebele, "Fiber grating sensors," J. Lightw. Technol., vol. 15, no. 8, pp. 1442–1463, Aug. 1997.

[11] T. Erdogan, "Fiber grating spectra", J. Lightw. Technol., vol. 15, no. 8, pp. 1277-1294, 1997.

[12] V. Bhatia, A. M. Vengsarkar, "Optical fiber long-period grating sensors", Optics Letters, vol. 21, no. 9, pp. 692-694, 1996.

[13] Q. Wu, Pak L. Chu, H. P. Chan, "General design approach to multi-channel fiber Bragg grating", J. Lightw. Technol., vol. 24, no. 3, 1571-1580, 2006.

[14] Q. Wu, G. Farrell and Y. Semenova, "Simple design technique for a triangular FBG filter based on a linearly chirped grating", Optics Communications 283, pp. 985-992, 2010.

[15] R. Slavík, J. Homola, and J. Ctyroký, "Single-mode optical fiber ˇ surface plasmon resonance sensor," Sens. Actuators B, Chem., vol. 54, nos. 1–2, pp. 74–79, Jan. 1999.

[16] A. K. Sharma, R. Jha, and B. D. Gupta, "Fiber-optic sensors based on surface plasmon resonance: a comprehensive review," IEEE Sensors Journal, vol. 7, no. 8, pp. 1118–1129, 2007.

[17] C. X. Teng, J. Zheng, Q. Y. Liang, S. J. Deng, H. C. Deng, H. Q. Liu, L. B. Yuan, "The Influence of Structural Parameters on the Surface Plasmon Resonance Sensor Based on a Side-Polished Macrobending Plastic Optical Fiber", IEEE Sensors Journal, vol. 20, no. 8, pp. 4245-4250, 2020.

[18] Q. Wu, Y. Semenova, P. Wang, and G. Farrell, "High sensitivity SMS fiber structure based refractometer – analysis and experiment," Opt. Express, vol. 19, no. 9, pp. 7937-7944, 2011.

[19] C. R. Liao, T. Y. Hu and D. N. Wang, "Optical fiber Fabry-Perot interferometer cavity fabricated by femtosecond laser micromachining and fusion splicing for refractive index sensing", Opt. Express, vol. 20, no. 20, pp. 22813-22818, 2012.

[20] D. A. Jackson, "Monomode optical fiber interferometers for precision measurement," Journal of Physics E Scientific Instruments, vol. 18, no. 12, pp. 981−1001, 1985.

[21] B. H. Lee, Y. H. Kim, K. S. Park, J. B. Eom, M. J. Kim, B. S. Rho and H. Y. Choi, "Interferometric Fiber Optic Sensors", Sensors, vol. 12, pp. 2467-2486, 2012.

[22] L. B. Soldano and E. C. M. Pennings, "Optical multi-mode interference devices based on self-imaging: Principles and applications," J. Lightwave Technol., vol. 13, pp. 615–627, 1995.

[23] T. Okamoto, I. Yamaguchi, "Multimode fiber-optic Mach-Zehnder interferometer and its use in temperature measurement", Applied Optics, vol. 27, no. 15, pp. 3085-3087, 1988.

[24] R. T. Cao, Y. Yang, Yang, M. H. Wang, X. R. Yi, J. Y. Wu, S. Huang, K. P. Chen, "Multiplexable intrinsic Fabry-Perot interferometric fiber sensors for multipoint hydrogen gas monitoring", Optics Letters, vol. 45, no. 11, 3163-3166, 2020.

[25] Y. J. Rao, "Recent progress in fiber-optic extrinsic Fabry Perot interferometric sensors", Opt. Fiber Technol., vol. 12, pp. 227-237, 2006.

[26] X. P. Zhang, L. X. Li, X. H. Zou, B. Luo, W. Pan, L. S. Yan and Q. Wu, "Angled fiber-based Fabry-Perot interferometer", Optics Letters, vol. 45, no.2, pp. 292-295, 2020.

[27] D. H. Kim, J. U. Kang, "Sagnac loop interferometer based on polarization maintaining photonic crystal fiber with reduced temperature sensitivity", Optics Letters, vol. 12, no. 19, pp. 4490-4495, 2004.

[28] E. Reyes-Vera, C. M. B. Cordeiro, P. Torres, "Highly sensitive temperature sensor using a Sagnac loop interferometer based on a side-hole photonic crystal fiber filled with metal", Applied Optics, vol. 56, no. 2, pp. 156-162, 2017.

[29] Q. Wang, G. Farrell and W. Yan, "Investigation on single-mode-multimode-single-mode fiber structure", Journal of Lightwave Technology, vol. 26, no. 5, pp. 512-519, 2008.

[30] S. M. Tripathi, A. Kumar, R. K. Varshney, et al., " Strain and Temperature Sensing Characteristics of Single-Mode-Multimode-Single-Mode Structures", Journal of Lightwave Technology, vol. 27, no. 13, pp. 2348-2356, 2009.

[31] D. P. Zhou, L. Wei, W. K. Liu, and J. W. Y. Lit, "Simultaneous strain and temperature measurement with fiber Bragg grating and multimode fibers using an intensity-based interrogation method," IEEE Photonics Technol. Lett., vol. 21, pp. 468–470, 2009.

[32] M. Kumar, A. Kumar, S. M. Tripathi, "A comparison of temperature sensing characteristics of SMS structures using step and graded index multimode fibers", Optics Communications, vol 312, pp. 222-226, 2014.

[33] O. Bryngdahl, Image formation using self-imaging techniques, J. Opt. Soc. Am., vol. 63, no. 4, pp. 416-419, 1973.

[34] Q. Wang, G. Farrell, T. Freir, "Study of transmission response of edge filters employed in wavelength measurements", Applied Optics, vol. 44, no. 36, pp. 7789-7792, 2005.

[35] A. M. Hatta, Y. Semenova, G. Farrell, "Performance evaluation of an all-fiber ratiometric wavelength monitor system using edge filters based on sms fiber structures", Microwave and Optical Technology Letters, vol. 55, no. 7, pp. 1645-1649, 2013.

[36] A. M. Hatta, Y. Semenova, G. Rajan, P. Wang, J. Zheng, G. Farrell, "Analysis of temperature dependence for a ratiometric wavelength measurement system using SMS fiber structure based edge filters", Optics Communications, vol. 283, no. 7, pp. 1291-1295, 2010.

[37] Q. Wu, Y. Semenova, G. Rajan, P. Wang and G. Farrell, "A study of the effect of source signal bandwidth on ratiometric wavelength measurement", Applied Optics, vol. 49, no. 29, pp. 5626-5631, 2010.

[38] Q. Wu, P. Wang, Y. Semenova, G. Farrell, "A study of the effect of the position of an edge filter within a ratiometric wavelength measurement", Measurement Science and Technology, vol. 21, no. 9, pp. 094013, 2010.

[39] A. M. Hatta, Y. Semenova, Q. Wu and G. Farrell, "Strain sensor based on a pair of single-mode– multimode–single-mode fiber structures in a ratiometric power measurement scheme", Applied Optics, vol. 49, no. 3, pp. 536-541, 2010.

[40] Q. Wu, A. M. Hatta, Y. Semenova and G. Farrell, "Use of a SMS fiber filter for interrogating FBG strain sensors with dynamic temperature compensation", Applied Optics, vol. 48, pp. 5451-5458, 2009.

[41] L. She, P. Wang, W. Sun, X. Wang, W. Yang, G. Brambilla, G. Farrell, "A Chalcogenide Multimode Interferometric Temperature Sensor Operating at a Wavelength of 2 μm", IEEE Sensors Journal, vol. 17, no. 6, pp. 1721-1726, 2017.

[42] Q. Wu, Y. Semenova, A. M. Hatta, P. Wang, G. Farrell, "Singlemode-Multimode-Singlemode fiber structures for simultaneous measurement of strain and temperature", Microwave and Optical Technology Letters, vol. 53, no. 9, pp. 2181-2185, 2011.

[43] A. M. Hatta, H. E. Permana, H. Setijono, A. K. Sekartedjo, "Strain measurement based on SMS fiber structure sensor and OTDR", Microwave and Optical Technology Letters, vol. 55, no. 11, pp. 2576-2678, 2013.

[44] P. Xu, Y. Dong, J. Zhang, D. Zhou, T. Jiang, J. Xu, H. Zhang, T. Zhu, Z. Lu, L. Chen, and X. Bao, "Bend-insensitive distributed sensing in singlemode-multimode-singlemode optical fiber structure by using Brillouin optical time-domain analysis", Optics Express, vol. 23, no. 17, pp. 22714-22722, 2015.

[45] Q. Wu, Y. Semenova, A. M. Hatta, P. Wang, G. Farrell, "Bent SMS fiber structure for temperature measurement", Electronic Letters, vol. 46, no.

16, pp. 1129-1130, 2010.
[46] R. T. Schermer, J. H. Cole, "Improved bend loss formula verified for optical fiber by simulation and experiment", J. Quantum Electronics, vol. 43, no. 10, pp. 899-909, 2007.
[47] Q. Wu, Y. Semenova, P. Wang, A. M. Hatta, G. Farrell, "Experimental demonstration of a simple displacement sensor based on a bent single-mode–multimode–single-mode fiber structure", Measurement Science and Technology, vol. 22, pp. 025203, 2011.
[48] Q. Wu, A. M. Hatta, P. Wang, Y. Semenova and G. Farrell, "Use of a Bent Single SMS Fiber Structure for Simultaneous Measurement of Displacement and Temperature Sensing", IEEE Photon. Tech. Lett., vol. 23, no. 2, pp. 130-132, 2011.
[49] S. Silva, O. Frazão, J. Viegas, L. A. Ferreira, F. M .Araújo, F. X. Malcata and J. L. Santos, "Temperature and strain-independent curvature sensor based on a singlemode/multimode fiber optic structure", Measurement Science and Technology, vol. 22, no. 8, pp. 085201, 2011.
[50] Y. Zhao, X.G. Li, F. C. Meng, Z. Zhao, "A vibration-sensing system based on SMS fiber structure", Sensors and Actuators A: Physical, vol. 214, pp. 163-167, 2014.
[51] Q. Wu, M. Yang, J. Yuan, H. P. Chan, Y. Ma, Y. Semenova, P. Wang, C. Yu and G. Farrell, "The use of a bend singlemode-multimode-singlemode (SMS) fiber structure for vibration sensing", Optics and Laser Technology, vol. 63, pp. 29-33, 2014.
[52] A. Z. Zulkifli, A. A. Latiff, M. C. Paul, M. Yasin, H. Ahmad, S. W. Harun, "Dual-wavelength nano-engineered Thulium-doped fiber laser via bending of singlemode-multimode-singlemode fiber structure", Optical Fiber Technology, vol. 32, pp. 96-101, 2016.
[53] N. H. Ysof, H. A. R. H. Arof, S. W. Harun, "Multimode interference in single mode - multimode - single mode fiber structure for steel beam compressive strain measurement", Microwave and Optical Technology Letters, vol. 60, no. 8, pp. 1971-1975, 2018.
[54] X. Li, D. Liu, R. Kumar, W. P. Ng, Y. Q. Fu, J. Yuan, C. Yu, Y. Wu, G. Zhou, G. Farrell, Y. Semenova, and Q. Wu, "A simple optical fiber interferometer based breathing sensor", Measurement Science and Technology, vol. 28, no. 3, 2017.
[55] R. Kumar, W. Han, D. Liu, W. P. Ng, R. Binns, K. Busawon, Y. Q. Fu, Z. Ghassemlooy, C. Underwood, K. Mahkamov, J. Yuan, C. Yu, H. Shu, X. A. Li, T. Guo, G. Farrell, Y. Semenova, and Q. Wu, "Optical fibre sensors for monitoring phase transitions in phase changing materials", Smart Materials and Structures, vol. 27, no. 10, 105021, 2018.
[56] J. W. Costa, M. A. R. Franco, V. A. Serao, C. M. B. Cordeiro, M. T. R. Giraldi, "Macrobending SMS fiber-optic anemometer and flow sensor", Optical Fiber Technology, vol. 52, pp. 101981, 2019.
[57] Q. Wang, Gerald Farrell, All-fiber multimode-interference-based refractometer sensor: proposal and design, Opt. Lett., vol. 31, no. 3, pp. 317–319, 2006.
[58] Y. Zhang, X. Tian, L. Xue, Q. Zhang, L. Yang, and B. Zhu, "Super-High Sensitivity of Fiber Temperature Sensor Based on Leaky-Mode Bent SMS Structure", Photon. Technol. Lett., vol. 25, no. 6, pp. 560-563, 2013.
[59] Y. Zhang, L. Xue, T. Wang, L. Yang, B. Zhu, and Q. Zhang, "High performance temperature sensing of single mode-multimode-single mode fiber with thermo-optic polymer as cladding of multimode fiber Segment", IEEE Sensors Journal, vol. 14, no. 4, pp. 1143-1147, 2014.
[60] W. Han, M. Rebow, X. Lian, D. Liu, G. Farrell, Q. Wu, Y. Ma, Y. Semenova, "SNS optical fiber sensor for direct detection of phase transitions in C18H38 n-alkane material", Experimental Thermal and Fluid Science, vol. 109, pp. 109854, 2019.
[61] Y. Zhao, L. Cai, X. G. Li, F. C. Meng, Z. Zhao, "Investigation of the high sensitivity RI sensor based on SMS fiber structure", Sensors and Actuators A: Physical, vol. 205, pp. 186-190, 2014.
[62] Z. B. Liu, Z. Tan, B. Yin, Y. Bai, S. Jian, "Refractive index sensing characterization of a singlemode–claddingless–singlemode fiber structure based fiber ring cavity laser", Optics Express, vol. 22, no. 5, pp. 5037-5042, 2014.
[63] X. Liu, X. Zhang, Y. Liu, Z. Liu, W. Peng, "Multi-point fiber-optic refractive index sensor by using coreless fibers", Optics Communications, vol. 365, pp. 168-172, 2016.
[64] L. Xue, D. Che, L. Yang, "High refractive index sensing based on single leaky mode attenuation", Optics Communications, vol. 294, pp. 198-201, 2013.
[65] I. D. Villar, J. Goni, A. Vicente, F. J. Arregui, and I. R. Matias, "Etched and Nanocoated Single-Mode Multimode Single-Mode (SMS) Fibers for Detection of Wind Turbine Gearbox Oil Degradation", Journal of Lightwave Technology, vol. 37, no. 18, pp. 4665-4673, 2019.
[66] E. E. Antúnez-Cerón1, M.A. Basurto-Pensado, A.R. Mejía-Aranda, R.J. Romero, J.J. Sánchez-Mondragón, H. H. Cerecedo-Núñez, A. Ochoa-Zezzati, "Estimation of LiBr-H2O Using Multimode Interference (MMI)", Journal of Applied Research and Technology, vol. 12, pp. 41-44, 2014.
[67] L. Xue and L. Yang, "Sensitivity Enhancement of RI Sensor Based on SMS Fiber Structure with High Refractive Index Overlay", Journal of Lightwave Technology, vol. 30, no. 10, pp. 1463-1469, 2012.
[68] I. D. Villar, A. B. Socorro, J. M. Corres, F. J. Arregui, and I. R. Matias, "Refractometric sensors based on multimode interference in a thin-film coated singlemode–multimode–single-mode structure with reflection configuration", Applied Optics, vol. 53, no. 18, pp. 3913-3919, 2014.
[69] I. D. Villar, A. B. Socorro, J. M. Corres, F. J. Arregui, and I. R. Matias, "Optimization of Sensors Based on Multimode Interference in Single-Mode–Multimode–Single-Mode Structure", Journal of Lightwave Technology, vol. 31, no. 22, pp. 3460-3468, 2013.
[70] A. B. Socorro, I. D. Villar, J. M. Corres, F. J. Arregui, and I. R. Matias "Sensitivity enhancement in a multimode interference-based SMS fibre structure coated with a thin-film: Theoretical and experimental study", Sensors and Actuators B: Chemical, vol. 190, pp. 363-369, 2014.
[71] A. B. Socorro, I. D. Villar, J. M. Corres, F. J. Arregui, and I. R. Matias, "Mode transition in complex refractive index coated single-mode–multimode–single-mode structure", Optics Express, vol. 21, no. 10, pp. 12668-12682, 2013.
[72] L. Li, Q. Han, Y. Chen, T. Liu, and R. Zhang, "An all-fiber optic current sensor based on ferrofluids and multimode interference", IEEE Sensors Journal, vol. 14, no. 6, pp. 1749-1753, 2014.
[73] R. Zhang, T. Liu, Q. Han, Y. Chen and L. Li, "U-bent single-mode-multimode-single-mode fiber optic magnetic field sensor based on magnetic fluid", Applied Physics Express, vol. 7, pp. 072501, 2014.
[74] X. Y. Wen, J. Huang, H. Xiao and M. H. Yang, "ZnO-coated SMS structure interrogated by a fiber ring laser for chemical sensing", Meas. Sci. Technol., vol. 25, pp. 114002, 2014.
[75] L. Singh, R. Singh, B. Zhang, B. K. Kaushik and S. Kumar, "Localized surface plasmon resonance based hetero-core optical fiber sensor structure for the detection of L-Cysteine", IEEE Transactions on Nanotechnology, vol. 19, pp. 201-208, 2020.
[76] A. Vicente, D. Santano, P. Zubiate, A. Urrutiaa, I. D. Villara, C. R. Zamarreño, "Lossy mode resonance sensors based on nanocoated multimode-corelessmultimode fibre", Sensors and Actuators B: Chemical, vol. 304, pp. 126955, 2020.
[77] Y. Cardona-Maya, A. B. Socorro, I. D. Villar, J. L. Cruz, J. M. Corres, J. F. Botero-Cadavid, "Label-free wavelength and phase detection based SMS fiber immunosensors optimized with cladding etching", Sensors and Actuators B: Chemical, vol 265, pp. 10-19, 2018.
[78] J. E. Antonio-Lopez, J. J. Sanchez-Mondragon, P. LiKamWa, D. A. May-Arrioja, "Fiber-optic sensor for liquid level measurement", Opt. Lett., vol. 36, no. 17, pp. 3425–3427, 2011.
[79] X. L. Zhou, K. Chen, X.F. Mao, W. Peng, Q. X. Yu, "A reflective fiber-optic refractive index sensor based on multimode interference in a coreless silica fiber", Opt. Commun., vol. 340, pp. 50-55, 2015.
[80] G. Zhou, Q. Wu, R. Kumar, W. P. Ng, H. Liu, L. Niu, N. Lalam, X. Yuan, Y. Semenova, G. Farrell, J. Yuan, C. Yu, J. Zeng, G. Y. Tian and Y. Q. Fu, "High sensitivity refractometer based on reflective SMF-small diameter no core fiber structure", Sensors vol. 17, pp. 1415-1424, 2017.
[81] S. Novais, C. I. A. Ferreira, M. S. Ferreira, J. L. Pinto, "Optical fiber tip sensor for the measurement of glucose aqueous solutions", IEEE Photonics J., vol. 10, no. 5, pp. 6803609, 2018.
[82] J. J. Zhu, A. P. Zhang, T. Hao Xia, S. He, W. Xue, "Fiber-Optic High-Temperature Sensor Based on Thin-Core Fiber Modal Interferometer", IEEE Sensors Journal, vol. 10, no. 9, pp. 1415-1418, 2010.
[83] J. Shi, S. Xiao, M. Bi, "In-series singlemode thin-core diameter fibres for simultaneous temperature and strain measurement", Electronics Letters, vol. 48, no. 2, pp. 93-U1195, 2012.
[84] B. Xu, J. Q. Li, Y. Li, X. Y. Dong, "A Thin-Core Fiber Modal Interferometer for Liquid-Level Sensing", Chinese Physics Letters, vol. 29, no. 10, pp. 104209, 2012.
[85] T. H. Xia, A. P. Zhang, B. Gu, J. J. Zhu, "Fiber-optic refractive-index sensors based on transmissive and reflective thin-core fiber modal interferometers", Optics Communications, vol. 283, pp. 2136-2139, 2010.

[86] Q. Wu, Y. Semenova, P. Wang, G. Farrell, "A comprehensive analysis verified by experiment of a refractometer based on an SMF28-Small-Core Singlemode fiber (SCSMF) -SMF28 fiber structure", Journal of Optics, vol. 13, no. 12, 125401, 2011

[87] M. Monerie, "Propagation in doubly clad single-mode fibers", IEEE Journal of quantum electronics, vol. QE-18, no. 4, pp. 535-542, 1982

[88] X. Lian, Q. Wu, G. Farrell, C. Shen, Y. Ma, Y. Semenova, "Discrete Self-Imaging in Small-Core Optical Fiber Interferometers", Journal of Lightwave Technology, vol. 3, no. 9, pp. 1873-1884, 2019.

[89] H. Fukano, T. Aiga, and S. Taue, "High-sensitivity fiber-optic refractive index sensor based on multimode interference using small-core single-mode fiber for biosensing", Japanese Journal of Applied Physics, vol. 53, pp. 04EL08, 2014.

[90] Q. Wu, Y. Semenova, J. Mathew, P. Wang and G. Farrell, "Humidity sensor based on a singlemode hetero-core fiber structure", Optics Letters, vol. 36, no, 10, pp. 1752-1754, 2011.

[91] B. Gu, M. J. Yin, A. P. Zhang, J. W. Qian, and S. He, "Low-cost high-performance fiber-optic pH sensor based on thin-core fiber modal interferometer", Optics Express, vol. 17, no. 25, pp. 22296-22302, 2009.

[92] B. Gu, M. J. Yin, A. P. Zhang, J. W. Qian, S. He, "Fiber-optic metal ion sensor based on thin-core fiber modal interferometer with nanocoating self-assembled via hydrogen bonding", Sensors and Actuators B: Chemical, vol. 160, pp. 1174-1179, 2011.

[93] M. Engholm, K. Hammarling, H. Andersson, M. Sandberg and H. E. Nilsson, "A Bio-Compatible Fiber Optic pH Sensor Based on a Thin Core Interferometric Technique", Photonics, vol. 6, no. 1, pp. 11, 2019.

[94] O. V. Ivanov, F. Yang, F. Tian, H. Du, "Thin-core fiber structures with overlays for sensing applications", Optics Express, vol. 25, no. 25, pp. 31197-31203, 2017.

[95] W. Yu, T. Lang, J. Bian, W. Kong, "Label-free fiber optic biosensor based on thin-core modal interferometer", Sensors and Actuators B: Chemical, vol. 228, pp. 322-329, 2016.

[96] X. Huang, X. Li, Y. Li, J. Yang, C. Tao, "Trace dissolved ammonia sensor based on porous polyelectrolyte membrane-coated thin-core fiber modal interferometer", Sensors and Actuators B: Chemical, vol. 226, pp. 7-13, 2016.

[97] X. Huang, X. Li, J. Yang, C. Tao, X. Guo, H. Bao, Y. Yin, H. Chen, Y. Zhu, "An in-line Mach-Zehnder Interferometer Using Thin-core Fiber for Ammonia Gas Sensing With High Sensitivity", Scientific Reports, vol. 7, pp. 44994, 2017.

[98] Y. Zheng, T. Lang, T. Shen, C. Shen, "Simple immunoglobulin G sensor based on thin core single-mode fiber", Optical Fiber Technology, vol. 41, pp. 104-108, 2018.

[99] S. C. Long, Y. R. Zhu, M. Y. Hu, Y. F. Qi, Y. R. Jiang, B. Liu and X. Zhang, "Thin-core fiber-optic biosensor for DNA hybridization detection", Optoelectronics Letters, vol. 14, no. 1, pp. 346-349, 2018.

[100] S. Liu, X. Yang, W. Feng, "Hydrogen sulfide gas sensor based on copper/graphene oxide coated multi-node thin-core fiber interferometer", Applied Optics, vol. 58, no. 9, pp. 2152-2157, 2019.

[101] Y. R. Wang, Z. Q. Tou, R. Ravikumar, Y. Y. Lim, Z. W. Ding, C. L. Zhao, P. L. So, and C. C. Chan, "Reflection-Based Thin-Core Modal Interferometry Optical Fiber Functionalized With PAA-PBA/PVA for Glucose Detection Under Physiological pH", Journal of Lightwave Technology, vol. 3, no. 11, pp. 2773-2777, 2019.

[102] P. Wang, K. Ni, B. Wang, Q. Ma, W. Tian, "Methylcellulose coated humidity sensor based on Michelson interferometer with thin-core fiber", Sensors and Actuators A: Physical, vol. 288, pp. 75-78, 2019.

[103] B. Wang, K. Ni, P. Wang, Q. Ma, W. Tian, L. Tan, "A CNT-coated refractive index sensor based on Michelson interferometer with thin-core fiber", Optical Fiber Technology, vol. 46, pp. 302-305, 2018.

[104] Q. F. Ma, Z. Q. Tou, K. Ni, Y. Y. Lim, Y. F. Lin, Y. R. Wang, M. H. Zhou, F. F. Shi, L. Niu, X. Y. Dong, C. C. Chan, "Carbon-nanotube Polyvinyl alcohol coated thin core fiber sensor for humidity measurement", Sensors and Actuators B: Chemical, vol. 257, pp. 800-806, 2018.

[105] M. A. Duguay, Y. Kokubun, T. L. Koch, and L. Pfeiffer, "Antiresonant reflecting optical waveguides in SiO_2-Si multilayer structures," Appl. Phys. Lett., vol. 49, no. 1, pp. 13-15, 1986.

[106] S. Liu, J. Tian, N. Liu, J. Xia, and P. Lu, "Temperature insensitive liquid level sensor based on antiresonant reflecting guidance in silica tube," J. Lightwave Technol., vol.34, no. 22, pp. 5239-5243, 2016.

[107] M. Hou, F. Zhu, Y. Wang, Y. Wang, C. Liao, S. Liu, and P. Lu, "Antiresonant reflecting guidance mechanism in hollow-core fiber for gas pressure sensing," Opt. Express, vol. 14, no. 14, pp. 27890-27898, 2016.

[108] D. Liu, Q. Wu, C. Mei, J. Yuan, X. Xin, A. K. Mallik, F. Wei, W. Han, R. Kumar, C. Yu, S. Wan, X. He, B. Liu, G. D. Peng, Y. Semenova, and G. Farrell, "Hollow Core Fiber Based Interferometer for High Temperature (1000 °C) Measurement", Journal of Lightwave Technology, vol. 36, no. 9, pp. 1583-1590, 2018

[109] A. M. Zheltikov, "Ray-optic analysis of the (bio)sensing ability of ring-cladding hollow waveguides," Appl. Opt., vol. 47, pp. 474–479, 2008.

[110] D. Liu, R. Kumar, F. Wei, W. Han, A. K. Mallik, J. Yuan, C. Yu, Z. Kang, F. Li, Z. Liu, H. Y. Tam, G. Farrell, Y. Semenova, and Q. Wu, "Highly sensitive twist sensor based on partially silver coated hollow core fiber structure", Journal of Lightwave Technology, vol. 36, no. 17, pp. 3672-3677, 2018.

[111] X. Zhang, H. Pan, H. Bai, M. Yan, J. Wang, C. Deng, T. Wang, "Transition of Fabry–Perot and antiresonant mechanisms via a SMF-capillary-SMF structure", vol. 43, no. 10, pp. 2268-2271, 2018.

[112] D. Liu, Q. Wu, W. Han, F. Wei, F. Ling, R. Kumar, A. K. Mallik, K. Tian, C. Shen, G. Farrell, Y. Semenova, P. Wang, "Strain independent twist sensor based on uneven platinum coated hollow core fiber structure", Optics Express, vol. 27, no. 14, pp. 19726-19736, 2019.

[113] N. Cai, L. Xia, Y. Wu, "Multiplexing of anti-resonant reflecting optical waveguides for temperature sensing based on quartz capillary", Optics Express, vol. 26, no. 5, pp. 33501-33509, 2018.

[114] R. Gao, Y. Jiang, and Y. Zhao, "Magnetic field sensor based on anti-resonant reflecting guidance in the magnetic gel-coated hollow core fiber," Opt. Lett., vol. 39, pp. 6293–6296, 2014.

[115] R. Gao, D. Lu, J. Cheng, Y. Jiang, L. Jiang, and Z. Qi, "Humidity sensor based on power leakage at resonance wavelengths of a hollow core fiber coated with reduced graphene oxide," Sens. Actuat. Biol. Chem., vol. 222, pp. 618–624, 2016.

[116] B. Xua, P. Li, D. N. Wang, C. L. Zhao, J. Dai, M. Yang, "Hydrogen sensor based on polymer-filled hollow core fiber with Pt-loaded WO3/SiO2 coating", Sensors and Actuators B: Chemical, vol 245, pp. 516-523, 2017.

[117] R. Gao, D. F. Lu, J. Cheng, Y. Jiang, L. Jiang, and Z. M. Qi, "Optical displacement sensor in a capillary covered hollow core fiber based on anti-resonant reflecting guidance," IEEE J. Sel. Top. Quantum Electron., vol. 23, pp. 5600106, 2017.

[118] D. Liu, F. Ling, R. Kumar, A. K. Mallik, K. Tian, C. Shen, G. Farrell, Y. Semenova, Q. Wu, P. Wang, "Sub-micrometer resolution liquid level sensor based on hollow core fiber structure", Optics Letters, vol. 44, no. 8, pp. 2125-2128, 2019.

[119] Z. Wu, B. Liu, J. Zhu, J. Liu, S. Wan, T. Wu and J. Sun, "Ultrahigh Resolution Thickness Measurement Technique Based on a Hollow Core Optical Fiber Structure", Sensors, vol. 20, pp. 2035, 2020.

[120] X. Zhang, H. Shao, Y. Yang, H. Pan, F. Pang, T. Wang, "Refractometry With a Tailored Sensitivity Based on a Single-Mode-Capillary-Single-Mode Fiber Structure", vol. 9, no. 2, pp. 6801908, 2017.

[121] X. Zhang, Y. Yang, H. Shao, H. Bai, F. Pang, H. Xiao, T. Wang, "Fano resonances in cone-shaped inwall capillary based microsphere resonator", Optics Express, vol. 25, no. 2, pp. 615-621, 2017.

[122] J. Wang, X. Zhang, M. Yan, L. Yang, F. Hou, W. Sun, X. Zhang, L. Yuan, H. Xiao, and T. Wang, "Embedded whispering-gallery mode microsphere resonator in a tapered hollow annular core fiber", Photonics Research, vol 6, no. 12, pp. 1124-1129, 2018.

[123] M. J. Kim, Y. M. Jung, B. H. Kim, W. T. Han, and B. H. Lee, "Ultra-wide bandpass filter based on long-period fiber gratings and the evanescent field coupling between two fibers," Opt. Express, vol. 15, no. 17, pp. 10855-10862, 2007.

[124] Q. Liu, K. S. Chiang, and Y. Q. Liu, "Analysis of Six-Port Optical Fiber Couplers Based on Three Parallel Long-Period Fiber Gratings," J. Lightwave Technol., vol. 26, pp. 3277-3286, 2008.

[125] Y. Q. Liu, K. S. Chiang, Y. J. Rao, Z. L. Ran, and T. Zhu, "Light coupling between two parallel CO2-laser written long-period fiber gratings," Opt. Express, vol. 15, no. 26, pp. 17645-17651, 2007.

[126] Z. Cai, F. Liu, T. Guo, B. O. Guan, G. D. Peng, and J. Albert, "Evanescently coupled optical fiber refractometer based a tilted fiber Bragg grating and a D-shaped fiber", Optics Express, vol. 23, no. 6, pp. 20971-20976, 2015.

[127] Y. M. Jung, G. Brambilla, G. S. Murugan, and D. J. Richardson, "Optical racetrack ring-resonator based on two U-bent microfibers," Appl. physics Lett., vol. 98, no. 2, pp. 021109, 2011.

[128] Z. H. Hong, X. W. Li, L. J. Zhou, X. W. Shen, J. G. Shen, S. G. Li, and J. P. Chen, "Coupling characteristics between two conical micro/nano

fibers: simulation and experiment," Opt. Express, vol. 19, no. 5, pp. 3854-3861, 2011.
[129] Y. Wu, X. Zeng, C. L. Hou, J. Bai, and G. G. Yang, "A tunable all-fiber filter based on microfiber loop resonator," Appl. Physics Lett., vol 92, no. 19, pp. 191112, 2008.
[130] Q. Wu, Y. Ma, J. Yuan, Y. Semenova, P. Wang, C. Yu, and G. Farrell, "Evanescent field coupling between two parallel close contact SMS fiber structures", Optics Express, vol. 20, no. 3, pp. 3098-3109, 2012.
[131] H. Kogelnik, R. V. Schmidt, "Switched directional couplers with alternating $\Delta\beta$," IEEE J. Quantum Electron. QE-12(7), pp. 396-401, 1976.
[132] K. S. Chiang, F. Y. M. Chan, and M. N. Ng, "Analysis of two parallel long-period fiber gratings," J. Lightwave Technol., vol. 22, no. 5, pp. 1358-1366, 2004.
[133] Q. Wu, Y. Semenova, Y. Ma, P. Wang, T. Guo, L. Jin and G. Farrell, "Light coupling between a singlemode- multimode-singlemode (SMS) fiber structure and a long period fiber grating", Journal of Lightwave Technology, vol. 29, no. 24, 3683-3688, 2011.
[134] Q. Wu, Y. Semenova, B. Yan, Y. Ma, P. Wang, C. Yu and G. Farrell, "Fiber refractometer based on a fiber Bragg grating and single-mode–multimode–single-mode fiber structure", Optics Letters, vol. 36, no. 12, pp. 2197-2199, 2011.
[135] Q. Rong, X. Qiao, T. Guo, R. Wang, J. Zhang, M. Hu, Z. Feng, Y. Weng, Y. Ma, "Temperature-calibrated fiber-optic refractometer based on a compact FBG-SMS structure", Chinese Optics Letters, vol. 3, pp. 030604, 2012.
[136] X. Wang, X. Dong, Y. Zhou, K. Ni, J. Cheng, and Z. Chen, "Hot-Wire Anemometer Based on Silver-Coated Fiber Bragg Grating Assisted by No-Core Fiber", Photonics Technology Letters, vol. 25, no. 24, pp. 2458-2461, 2013.
[137] Q. Wu, H. P. Chan, Jinhui Yuan, Youqiao Ma, Minwei Yang, Yuliya Semenova, Binbin Yan, Pengfei Wang, Chongxiu Yu and Gerald Farrell, "Enhanced refractive index sensor using a combination of a long period fiber grating and a small core singlemode fiber structure", Measurement Science and Technology, vol. 24, pp. 094002, 2013.
[138] M. Ding, B. Yang, P. Jiang, X. Liu, L. Dai, Y. Hu, B. Zhang, "High-sensitivity thermometer based on singlemode-multimode FBG-singlemode fiber", Optics and Laser Technology, vol. 96, pp. 313-317, 2017.
[139] A. Sun and Z. Wu, "Multimode Interference in Single Mode–Multimode FBG for Simultaneous Measurement of Strain and Bending", IEEE Sensors Journal, vol. 15, no. 5, pp. 3390-3394, 2015.
[140] D. Song, Q. Chai, Y. Liu, Y. Jiang, J. Zhang, W. Sun, L. Yuan, J. Canning and G. D. Peng, "A simultaneous strain and temperature sensing module based on FBG-in-SMS", Meas. Sci. Technol., vol. 25, pp. 055205, 2014.
[141] H. Lin, F. Liu, Y. Dai, A. Zhou, "Cascaded Fiber Mach–Zehnder Interferometers for Sensitivity-Enhanced Gas Pressure Measurement", IEEE Sensors Journal, vol. 19, no. 7, pp. 2581-2586, 2019.
[142] H. Sakata, F. Kosaka, M. Kubota, R. Kimbara, and K. Okada, "Tunable Tm/Ho-codoped fiber lasers based on an extensible liquid core between a pair of fused multimode-single-mode fibers," Appl. Opt., vol. 58, pp. 5288-5293, 2019.
[143] B. Yin, Y. Li, Z. B. Liu, S. Feng, Y. Bai, Y. Xu, S. Jian, "Investigation on a compact in-line multimode-single-mode-multimode fiber structure", Optics and Laser Technology, vol. 80, pp. 16-21, 2016.
[144] Y. Zhang, A. Zhou, B. Qin, H. Deng, Z. Liu, J. Yang, and L. Yuan, "Refractive Index Sensing Characteristics of Single-Mode Fiber-Based Modal Interferometers", Journal of Lightwave Technology, vol. 32, no. 9, pp. 1734-1740, 2014.
[145] Y. Zhao, L. Cai, X. G. Li, "High sensitive modal interferometer for temperature and refractive index measurement", Photonics Technology Letters, vol. 27, no. 12, pp. 1341-1344, 2015.
[146] H. Gao, Y. Jiang, Y. Cui, L. Zhang, J. Jia and J. Hu, "Dual-Cavity Fabry–Perot Interferometric Sensors for the Simultaneous Measurement of High Temperature and High Pressure," IEEE Sensors Journal, vol. 18, no. 24, pp. 10028-10033, 2018.
[147] X. Li, L. V. Nguyen, M. Becker, H. Ebendorff-Heidepriem, D. Pham and S. C. Warren-Smith, "Simultaneous Measurement of Temperature and Refractive Index Using an Exposed Core Microstructured Optical Fiber," IEEE Journal of Selected Topics in Quantum Electronics, vol. 26, no. 4, pp. 1-7, 2020.
[148] Q. Wu, Y. Semenova, P. Wang and G. Farrell, "Fibre heterostructure for simultaneous strain and temperature measurement," *Electronics Letters*, vol. 47, no. 12, pp. 713 -714, 2011.
[149] N. Bhatia and J. John, "Multimode interference devices with single-mode–multimode–multimode fiber structure," Appl. Opt., vol. 53, pp. 5179-5186, 2014.
[150] N. Bhatia and J. John, "Single-mode–multimode–multimode device: sensitivity of the single mode to the fiber parameters and geometrical misalignments," J. Opt. Soc. Am. B, vol. 33, pp. 211-219, 2016.
[151] L. Li, L. Xia, Z. Xie, and D. Liu, "All-fiber Mach-Zehnder interferometers for sensing applications," Opt. Express, vol. 20, pp. 11109-11120, 2012.
[152] M. Shao, X. Qiao, H. Fu, H. Li, Z. Jia and H. Zhou, "Refractive Index Sensing of SMS Fiber Structure Based Mach-Zehnder Interferometer," IEEE Photonics Technology Letters, vol. 26, no. 5, pp. 437-439, 2014.
[153] Y. Miao, H. Zhang, J. Lin, B. Song, K. Zhang, W. Lin, B. Liu, and J. Yao, "Simultaneous measurement of temperature and magnetic field based on a long period grating concatenated with multimode fiber," Appl. Phys. Lett., vol. 106, no. 13, pp. 132410, 2015.
[154] J. Zhang, S. Pu, J. Rao, T. Yao, "Refractive index and temperature sensors based on no-core fiber cascaded with long period fiber grating", Journal of Modern Optics, vol. 65, no. 9, pp. 1098-1103, 2018.
[155] D. Monzón-Hernández, A. Martínez-Ríos, G. Salceda-Delgado and J. Villatoro, "Compact Sensors Based on Cascaded Single-Mode–Multimode–Single-Mode Fiber Structures", Applied Physiscs Express, vol. 6, no. 3, pp. 032502, 2013.
[156] S. Zhang, S. Deng, Z. Wang , C. Sun, X. Chen, Y. Ma, L. Zhao, C. Lu, T. Geng, W. Yang, L. Yuan, "A miniature SMS-LPG bending sensor with high sensitivity based on multimode fiber embedded-LPG", Sensors and Actuators A: Physical, vol. 295, pp. 31-36, 2019.
[157] S. Zhang, S. Deng, Z. Wang, W. Yang, Cuiting Sun, X. Chen, Y. Ma, Y. Li, T. Geng, W. Sun, and L. Yuan, "Optimization and experiment of a miniature multimode fiber induced-LPG refractometer," OSA Continuum, vol. 2, pp. 2190-2198, 2019.
[158] S. Zhang, T. Geng, H. Niu, X. Li, Y. Yan, C. Sun, S. Deng, Z. Wang, S. Wang, W. Yang, W. Sun, and L. Yuan, "All fiber compact bending sensor with high sensitivity based on a multimode fiber embedded chirped long-period grating," Opt. Lett., vol. 45, pp. 4172-4175, 2020.
[159] P. Wang, S. Zhang, R. Wang, G. Farrell, M. Zhang, T. Geng, E. Lewis, and K. Tian, "Temperature-insensitive refractometer based on an RI-modulated singlemode-multimode-singlemode fibre structure," Opt. Express, vol. 27, pp. 13754-13764, 2019.
[160] G. Zhou, R. Kumar, Q. Wu, W. P. Ng, R. Binns, N. Lalam, X. Miao, L. Niu, X. Yuan, Y. Semenova, G. Farrell, J. Yuan, C. Yu, X. Sang, X. Xin, B. Liu, H. Lv, Y. Q. Fu, "A simple all-fiber comb filter based on the combined effect of multimode interference and Mach-Zehnder interferometer", Scientific Reports, vol. 8, pp. 11803, 2018
[161] B. Jiang et al., "Fano-Like Resonance in an All-in-Fiber Structure," IEEE Photonics Journal, vol. 11, no. 5, pp. 1-7, 2019.
[162] J. Chen, J. Zhou and Z. Jia, "High-Sensitivity Displacement Sensor Based on a Bent Fiber Mach–Zehnder Interferometer," in IEEE Photonics Technology Letters, vol. 25, no. 23, pp. 2354-2357, 2013.
[163] R. Q. Lv, J. K. Qian, Y. Zhao, "Magnetic field sensor based on the magnetic-fluid-clad combined with singlemode–multimode–singlemode fiber and large core-offset splicing structure", Measurement Science and Technology, vol. 29, no. 3, pp. 035204, 2018.
[164] W. Han, Z. Tong, Y. Cao, "Simultaneous measurement of temperature and liquid level base on core-offset singlemode–multimode–singlemode interferometer", Optics Communications, vol. 321, pp. 134-137, 2014.
[165] K. Zhang, I. Alamgir and M. Rochette, "Midinfrared Compatible Tunable Bandpass Filter Based on Multimode Interference in Chalcogenide Fiber," in Journal of Lightwave Technology, vol. 38, no. 4, pp. 857-863, 2020.
[166] X. Fan, J. Jiang, X. Zhang, K. Liu, S. Wang, and T. Liu, "Multimode interferometer-based torsion sensor employing perfluorinated polymer optical fiber," Opt. Express, vol. 27, pp. 28123-28132, 2019.
[167] F. Wang, K. Pang, T. Ma, X. Wang, H. Lu, Y. Liu, "S-shaped refractometer based on dual tapered no-core fiber for low-range refractive index measurement", Optics Communications, vol. 463, pp. 125419, 2020.
[168] K. Tian, M. Zhang, G. Farrell, R. Wang, E. Lewis, and P. Wang, "Highly sensitive strain sensor based on composite interference established within S-tapered multimode fiber structure," Opt. Express, vol. 26, pp. 33982-33992, 2018.
[169] H. Ahmad, S. N. Aidit, S. I. Ooi and Z. C. Tiu, "Supercontinuum Micrometer-Displacement Sensor Using Single-Multi-Air-Gap-Single Mode Fiber as Sensing Probe," IEEE Sensors Journal, vol. 18, no. 20, pp. 8275-8279, 2018.

[170] K. Tian, G. Farrell, X. Wang, W. Yang, Y. Xin, H. Liang, E. Lewis, and P. Wang, "Strain sensor based on gourd-shaped single-mode-multimode-single-mode hybrid optical fibre structure," Opt. Express 25, 18885-18896 (2017)

[171] Y. Li, P. Lu, Z. Qu, W. Zhang, W. Ni, D. Liu, J. Zhang, "An Optical Fiber Twist Sensor With Temperature Compensation Mechanism Based on T-SMS Structure," in IEEE Photonics Journal, vol. 12, no. 1, pp. 1-8, 2020.

[172] T. Jiao, H. Meng, S. Deng, S. Liu, X. Wang, Z. Wei, F. Wang, C. Tan, X. Huang, "Simultaneous measurement of refractive index and temperature using a Mach-Zehnder interferometer with forward core-cladding-core recoupling", Optics & Laser Technology, vol. 111, pp. 612-615, 2019.

[173] J. An, Y. Jin, M. Sun and X. Dong, "Relative Humidity Sensor Based on SMS Fiber Structure With Two Waist-Enlarged Tapers," in IEEE Sensors Journal, vol. 14, no. 8, pp. 2683-2686, 2014.

[174] F. Liu, H. F. Lin, Y. Liu, A. Zhou, and Y. T. Dai, "Femtosecond-induced spiral micro-structured SMS fiber structure for refractive index measurement," Opt. Express, vol. 26, pp. 17388-17396, 2018.

[175] C. Zhang, T. Ning, J. Li, J. Zheng, X. Gao, L. Pei, "Refractive index and strain sensor based on twin-core fiber with a novel T-shaped taper", Optics & Laser Technology, vol. 102, pp. 12-16, 2018.

[176] L. Hou, X. Zhang, J. Yang, J. Kang, L. Ran, "Simultaneous measurement of refractive index and temperature based on half-tapered SMS fiber structure with fringe-visibility difference demodulation method", Optics Communications, vol. 433, pp. 252-255, 2019.

[177] Y. C. Liao, B. Liu, J. Liu, S. P. Wan, X. D. He, J. Yuan, X. Fan and Q. Wu, "High Temperature (Up to 950 °C) Sensor Based on Micro Taper In-Line Fiber Mach–Zehnder Interferometer", Applied Sciences-Basel, vol. 9, no. 12, pp. 2394, 2019.

[178] P. Zhang *et al*., "Investigation of a Side-Polished Fiber MZI and Its Sensing Performance," in *IEEE Sensors Journal*, vol. 20, no. 11, pp. 5909-5914, 2020.

[179] J. C. Knight, G. Cheung, F. Jacques, and T. A. Birks, "Phase-matched excitation of whispering-gallery-mode resonances by a fiber taper," Opt. Lett., vol. 22, no. 15, pp. 1129–1131, 1997.

[180] L. Tong et al., "Subwavelength-diameter silica wires for low-loss optical wave guiding," Nature, vol. 426, no. 6968, pp. 816–819, 2003.

[181] S. Lacroix, F. Gonthier, R. J. Black, and J. Bures, "Tapered-fiber interferometric wavelength response: the achromatic fringe," Opt. Lett., vol. 13, pp. 395-397, 1988.

[182] O. Frazão, P. Caldas, F. M. Araújo, L. A. Ferreira, and J. L. Santos, "Optical flowmeter using a modal interferometer based on a single nonadiabatic fiber taper," Opt. Lett., vol. 32, pp. 1974-1976, 2007.

[183] G. Salceda-Delgado, et al., "Optical microfiber mode interferometer for temperature-independent refractometric sensing", Opt. Lett., vol. 37, no. 11, pp. 1974–1976, 2012.

[184] H. Luo, Q. Sun, Z. Xu, D. Liu, and L. Zhang, "Simultaneous measurement of refractive index and temperature using multimode microfiber-based dual Mach–Zehnder interferometer," Opt. Lett., vol. 39, pp. 4049-4052, 2014.

[185] L. Xu, Y. Li, B. Li, "Nonadiabatic fiber taper-based Mach-Zehnder interferometer for refractive index sensing", Appl. Phys. Lett., vol. 101 no. 15, pp. 153510, 2012.

[186] W. B. Ji, Y. C. Tan, B. Lin, S. C. Tjin, K. K. Chow, "Nonadiabatically tapered microfiber sensor with ultrashort waist", Photonics Technol. Lett., vol. 26, no. 22, 2303-2306, 2014.

[187] H. Luo, Q. Sun, Z. Xu, W. Jia, D. Liu and L. Zhang, "Microfiber-Based Inline Mach–Zehnder Interferometer for Dual-Parameter Measurement," IEEE Photonics Journal, vol. 7, no. 2, pp. 1-8, 2015.

[188] A.B. Socorro, I. Del Villar, J.M. Corres, F.J. Arregui, I.R. Matias, "Spectral width reduction in lossy mode resonance-based sensors by means of tapered optical fibre structures", Sensors and Actuators B: Chemical, vol. 200, pp. 53-60, 2014.

[189] Y. Li, H. Ma, L. Gan, Q. Liu, Z. Yan, D. Liu, Q. Sun, "Immobilized optical fiber microprobe for selective and high sensitive glucose detection", Sensors and Actuators B: Chemical, vol. 255, pp. 3004-3010, 2018.

[190] L. P. Sun, Y. Huang, T. Huang, Z. Yuan, W. Lin, Z. Sun, M. Yang, P. Xiao, J. Ma, W. Wang, Y. Zhang, Z. Liu, and B. O. Guan, "Optical Microfiber Reader for Enzyme-Linked Immunosorbent Assay", Analytical Chemistry, vol. 91, no. 21, pp. 14141-14148, 2019.

[191] A. Xiao, Y. Huang, J. Zheng, P. Chen, and B. O. Guan, "An Optical Microfiber Biosensor for CEACAM5 Detection in Serum: Sensitization by a Nanosphere Interface", ACS Applied Materials & Interfaces, vol. 12, no. 1, pp. 1799-1805, 2020.

[192] Y. Huang, P. Chen, H. Liang, A. Xiao, S. Zeng, B. O. Guan, "Nucleic acid hybridization on a plasmonic nanointerface of optical microfiber enables ultrahigh-sensitive detection and potential photothermal therapy", Biosensors and Bioelectronics, vol. 156, pp. 112147, 2020.

[193] H. Li, Y. Huang, G. Hou, A. Xiao, P. Chen, H. Liang, Y. Huang, X. Zhao, L. Liang, X. Feng and B. O. Guan, "Single-molecule detection of biomarker and localized cellular photothermal therapy using an optical microfiber with nanointerface", Science Advances, vol. 5, no. 12, pp. eaax4659, 2019.

[194] P. Wang, G. Brambilla, M. Ding, Y. Semenova, Q. Wu, G. Farrell, "A high sensitivity, evanescent field refractometric sensor based on tapered multimode fiber interference", Optics Letters, vol. 36, no. 12, pp. 2233-2235, 2011.

[195] P. Wang, M. Ding, L. Bo, C. Guan, Y. Semenova, Qiang Wu, G. Farrell and G. Brambilla, "A fiber tip high temperature sensor based on multimode interference," Optics Letters, Vol. 38, No. 22, pp. 4617-4620, 2013.

[196] Y. Zhang, W. Zou, X. Li, J. Mao, W. Jiang, and J. Chen, "Modal interferometer based on tapering single-mode-multimode-single-mode f iber structure by hydrogen flame," Chin. Opt. Lett., vol. 10, pp. 070609-070609, 2012.

[197] R. Gao, H. Wang, D. Zhu, G. Fan, H. Yan, P. Wang, Y. Liu, Y. Wang, W. Liu, L. Song, C. Wang, Y. Chen, "Acoustic frequency vibration sensor based on tapered SMS fiber structure", Sensors and Actuators A: Physical, vol. 271, pp. 243-250, 2018.

[198] L. P. Sun, J. Li, S. Gao, L. Jin, Y. Ran, and B. O. Guan, "Fabrication of elliptic microfibers with CO2 laser for high-sensitivity refractive index sensing," Opt. Lett., vol. 39, pp. 3531-3534, 2014.

[199] B. Yang, Y. Niu, B. Yang, Y. Hu, L. Dai, Y. Yin, M. Ding, "High sensitivity balloon-like refractometric sensor based on singlemode-tapered multimode-singlemode fiber", Sensors and Actuators A: Physical, vol. 281, pp. 42-47, 2018.

[200] X. Wang, K. Tian, L. Yuan, E. Lewis, G. Farrell and P. Wang, "A High-Temperature Humidity Sensor Based on a Singlemode-Side Polished Multimode-Singlemode Fiber Structure," Journal of Lightwave Technology, vol. 36, no. 13, pp. 2730-2736, 2018.

[201] J. Shi, S. Xiao, L. Yi, M. Bi, "A Sensitivity-Enhanced Refractive Index Sensor Using a Single-Mode Thin-Core Fiber Incorporating an Abrupt Taper", *Sensors, vol. 12, pp.* 4697-4705, 2012.

[202] D. Liu, A. K. Mallik, J. Yuan, C. Yu, G. Farrell, Y. Semenova, Q. Wu, "High sensitivity refractive index sensor based on a tapered small core single-mode fiber structure", Optics Letters, vol. 40, no. 17, pp. 4166-4169, 2015.

[203] D. Liu, W. Han, A. K. Mallik, J. Yuan, C. Yu, G. Farrell, Y. Semenova, and Q. Wu, "High sensitivity sol-gel silica coated optical fiber sensor for detection of ammonia in water", Optics Express, Vol. 24, no.21, pp. 24179-24187, 2016.

[204] D. Liu, R. Kumar, F. Wei, W. Han, A. K. Mallik, J. Yuan, S. Wan, X. He, Z. Kang, F. Li, C. Yu, G. Farrell, Y. Semenova and Q. Wu, "High sensitivity optical fiber sensors for simultaneous measurement of methanol and ethanol", Sensors and Actuators B: Chemical, vol. 271, pp. 1-8, 2018.

[205] X. Zhang *et al*., "Label-Free Detection of DNA Hybridization Utilizing Dual S-Tapered Thin-Core Fiber Interferometer," Journal of Lightwave Technology, vol. 37, no. 11, pp. 2762-2767, 2019.

[206] W.F. de Morais, M.T.M.R. Giraldi, "Comparative performance analysis of relative humidity sensor based on intermodal interference using tapered square no-core optical fiber and tapered cylindrical optical fiber", Opt Quant Electron., vol. 51, pp. 288, 2019.

[207] K. Tian, G. Farrell, X. Wang, Y. Xin, Y. Du, W. Yang, H. Liang, E. Lewis, P. Wang, "High sensitivity temperature sensor based on singlemode-no-core-singlemode fibre structure and alcohol", Sensors and Actuators A: Physical, vol. 284, pp. 28-34, 2018.

[208] M. Zhang, G. Zhu, L. Lu, X. Lou, L. Zhu, "Refractive index sensor based on ultrafine tapered single-mode nocladding single-mode fiber structure", Optical Fiber Technology, vol. 48, pp. 297-302, 2019.

[209] F. Wang, K. Pang, T. Ma, X. Wang, Y. Liu, "Folded-tapered multimode-no-core fiber sensor for simultaneous measurement of refractive index and temperature", Optics & Laser Technology, vol. 130, pp. 106333, 2020.

[210] R. Kumar, Y. Leng, B. Liu, J. Zhou, L. Shao, J. Yuan, X. Fan, S. Wan, T. Wu, J. Liu, R. Binns, Y. Q. Fu, W. P. Ng, G. Farrell, Y. Semenova, H. Xu, Y. Xiong, X. He and Q. Wu, "Ultrasensitive biosensor based on magnetic microspheres enhanced microfiber interferometer", Biosensors & Bioelectronics, vol. 145, pp. 111563, 2019.

[211] Y. Zhao, F. Xia, M. Q. Chen, R. Q. Lv, “Optical fiber low-frequency vibration sensor based on Butterfly-Shape Mach-Zehnder Interferometer”, Sensors and Actuators A: Physical, vol. 273, pp. 107-112, 2018.
[212] L. Chen et al., "Novel Microfiber Sensor and Its Biosensing Application for Detection of hCG Based on a Singlemode-Tapered Hollow Core-Singlemode Fiber Structure," IEEE Sensors Journal, vol. 20, no. 16, pp. 9071-9078, 2020.
[213] X. Zhan, Y. Liu, M. Tang, L. Ma, R. Wang, L. Duan, L. Gan, C. Yang, W. Tong, S. Fu, D. Liu, and Z. He, "Few-mode multicore fiber enabled integrated Mach-Zehnder interferometers for temperature and strain discrimination," Opt. Express, vol. 26, pp. 15332-15342, 2018.
[214] M. Yang, J. Yang, C. Guan, M. Wang, P. Geng, Yize Shen, J. Zhang, J. Shi, J. Yang, and L. Yuan, "Refractive index sensor based on etched eccentric core few-mode fiber dual-mode interferometer," Opt. Express, vol. 27, pp. 28104-28113, 2019.
[215] B. Sun, F. Fang, Z. Zhang, J. Xu, and L. Zhang, "High-sensitivity and low-temperature magnetic field sensor based on tapered two-mode fiber interference," Opt. Lett., vol. 43, pp. 1311-1314, 2018.
[216] J. Li, M. Geng, L. P. Sun, P. Fan, B. Liu, and B. O. Guan, "Investigation on single taper-based all-solid photonic bandgap fiber modal interferometers," Opt. Express, vol. 24, pp. 8547-8554, 2016.
[217] X. Li, N.-K. Chen, L. Xi, H. Zhang, X. Zhang, W. Zhang, and X. Tang, "Micro-fiber Mach–Zehnder interferometer based on ring-core fiber," Opt. Express, vol. 27, pp. 34603-34610, 2019.
[218] H. Fu, Q. Wang, J. Ding, Y. Zhu, M. Zhang, C. Yang, S. Wang, “Fe2O3 nanotube coating micro-fiber interferometer for ammonia detection”, Sensors and Actuators B: Chemical, vol. 303, pp. 127186, 2020.
[219] X. Wang, J. Zhang, K. Tian, S. Wang, L. Yuan, E. Lewis, G. Farrell, and P. Wang, "Investigation of a novel SMS fiber based planar multimode waveguide and its sensing performance," Opt. Express, vol. 26, pp. 26534-26543, 2018.
[220] S. Li, Y. Zhao, “A Mach-Zehnder interferometer based on tapered dual side hole fiber for refractive index sensing”, Optical Fiber Technology, vol. 45, pp. 267-270, 2018.
[221] Y. Zhao, L. Cai and H. Hu, "Fiber-Optic Refractive Index Sensor Based on Multi-Tapered SMS Fiber Structure," *IEEE Sensors Journal*, vol. 15, no. 11, pp. 6348-6353, 2015.
[222] P. Wang *et al*., "Enhanced Refractometer Based on Periodically Tapered Small Core Singlemode Fiber," in *IEEE Sensors Journal*, vol. 13, no. 1, pp. 180-185, Jan. 2013.
[223] B. S. Kawasaki and K. O. Hill, “Low-loss access coupler for multimode optical fiber distribution networks,” Appl. Opt., vol. 16, no. 7, pp. 1794–1795, 1977.
[224] B. S. Kawasaki, K. O. Hill, R. G. Lamont, “Biconical-taper single-mode fiber coupler”, Optics Letters, vol. 6, no. 7, pp. 327-328, 1981.
[225] Y. Jung, G. Brambilla, and D. J. Richardson, “Optical microfiber coupler for broadband single-mode operation,” Opt. Express, vol. 17, no. 7, pp. 5273–5278, 2009.
[226] P. Wang et al., “High temperature performance of an optical microfibre coupler and its potential use as a sensor,” Electron. Lett., vol. 48, no. 5, pp. 283–284, 2012.
[227] M. Ding, P. Wang, and G. Brambilla, “A microfiber coupler tip thermometer,” Opt. Express, vol. 20, no. 5, pp. 5402–5408, 2012.
[228] S. Pu, L. Luo, J. Tang, L. Mao, and X. Zeng, “Ultrasensitive refractiveindex sensors based on tapered fiber coupler with Sagnac loop,” IEEE Photon. Technol. Lett., vol. 28, no. 10, pp. 1073–1076, May 2016.
[229] Q. Zhang, J. Lei, B. Cheng, Y. Song, L. Hua, and H. Xiao, “A microfiber half coupler for refractive index sensing,” IEEE Photon. Technol. Lett., vol. 29, no. 18, pp. 1525–1528, Sep. 2017.
[230] M. V. Hernandez-Arriaga, M. A. Bello-Jim´enez, A. Rodr´ıguez-Cobos, and R. L´opez-Estopier, “High sensitivity refractive index sensor based on highly overcoupled tapered fiber-optic couplers,” IEEE Sensors J., vol. 17, no. 2, pp. 333–339, Jan. 2017.
[231] Y. Chen, S.-C.Yan, X. Zheng, F. Xu, and Y.-Q. Lu, “A miniature reflective micro-force sensor based on a microfiber coupler,” Opt. Express, vol. 22, no. 3, pp. 2443–2450, 2014.
[232] S. C. Yan, Z. Y. Liu, C. Li, S. J. Ge, F. Xu, and Y. Q. Lu, “Hot-wire microfluidic flowmeter based on a microfiber coupler,” Opt. Lett., vol. 41, no. 24, pp. 5680–5683, 2016.
[233] S. C. Yan, Y. Chen, C. Li, F. Xu, and Y. Q. Lu, “Differential twin receiving fiber-optic magnetic field and electric current sensor utilizing a microfiber coupler,” Opt. Express, vol. 23, no. 7, pp. 9407–9414, 2015.
[234] L. Luo et al., “Highly sensitive magnetic field sensor based on microfiber coupler with magnetic fluid,” Appl. Phys. Lett., vol. 106, no. 19, pp. 193507, 2015.
[235] F. Wei, A. K. Mallik, D. Liu, Q. Wu, G. D. Peng, G. Farrell & Y. Semenova, “Magnetic field sensor based on a combination of a microfiber coupler covered with magnetic fluid and a Sagnac loop”, Scientific Reports, vol. 7, no. 1, 4725, 2017.
[236] F. Wei, D. Liu, A. K. Mallik, G. Farrell, Q. Wu, G. D. Peng, Y. Semenova, “Temperature-compensated magnetic field sensing with a dual-ring structure consisting of microfiber coupler-Sagnac loop and fiber Bragg grating-assisted resonant cavity”, Applied Optics, vol. 58, no. 9, 2334-2339, 2019.
[237] F. Wei, D. Liu, A. K. Mallik, G. Farrell, Q. Wu, G. D. Peng, Y. Semenova, “Magnetic Field Sensor Based on a Tri-Microfiber Coupler Ring in Magnetic Fluid and a Fiber Bragg Grating”, Sensors, vol. 19, no. 23, pp. 5100, 2020.
[238] L. Sun, Y. Semenova, Q. Wu, D. Liu, J. Yuan, X. Sang, B. Yan, K. Wang, C. Yu, and G. Farrell, “Investigation of humidity and temperature response of a silica gel coated microfiber coupler”, Photonics Journal, vol. 8, no. 6, pp. 6805407, 2016.
[239] Y. Peng, Y. Zhao, X. Hu, M. Chen, “Humidity sensor based on unsymmetrical U-shaped twisted microfiber coupler with wide detection range”, Sensors and Actuators B: Chemical, vol. 290, pp. 406-413, 2019.
[240] D. R. Li et al., “Ethanol gas sensor based on a hybrid polymethyl methacrylate-silica microfiber coupler,” J. Lightw. Technol., vol. 36, no. 10, pp. 2031–2036, May 2018.
[241] L. Sun, Y. Semenova, Q. Wu, D. Liu, J. Yuan, Tao Ma, X. Sang, B. Yan, K. Wang, C. Yu, and G. Farrell, “High sensitivity ammonia gas sensor based on a silica gel coated microfiber coupler”, Journal of Lightwave Technology, pp. 2864-2870, vol. 35, no. 14, 2017.
[242] K. Li, N. Zhang, N. M. Y. Zhang, W. Zhou, T. Zhang, M. Chen, L. Wei, “Birefringence induced Vernier effect in optical fiber modal interferometers for enhanced sensing”, Sensors and Actuators B: Chemical, vol. 275, pp. 16-24, 2018.
[243] G. Zhou, L. Niu, Y. Jiang, H. Liu, X. Xie, H. Yan, L. Yan, J. Liu, J. Chen, X. Miao, H. Zhou, X. Jiang, H. Lv, “Sensing of airborne molecular contaminants based on microfiber coupler with mesoporous silica coating”, Sensors and Actuators A: Physical, vol. 287, pp. 1-7, 2019.
[244] W. Zhou, K. Li, Y. Wei, P. Hao, M. Chi, Y. Liu, Y. Wu, “Ultrasensitive label-free optical microfiber coupler biosensor for detection of cardiac troponin I based on interference turning point effect”, Biosensors and Bioelectronics, vol. 106, pp. 99-104, 2018.
[245] L. Chen, Y. K. Leng, B. Liu, J. Liu, S. P. Wan, T. Wu, J. Yuan, L. Shao, G. Gu, Y. Q. Fu, H. Xu, Y. Xiong, X. D. He and Q. Wu, “Ultrahigh-sensitivity label-free optical fiber biosensor based on a tapered singlemode-no core-singlemode coupler for Staphylococcus aureus detection”, Sensors and Actuators B: Chemical, vol. 320, pp. 128283, 2020.
[246] Z. Wu, B. Liu, J. Zhu, J. Liu, S. Wan, T. Wu, J. Sun, “Asymmetrical tapered SMS fiber coupler for simultaneous measurement of temperature and refractive index and its application for biosensing”, Chinese Optics Letters, vol. 18, no. 6, pp. 061201, 2020.